esa esrin

european space agency
agence spatiale européenne

ERS-1 SAR Antenna Pattern Estimation

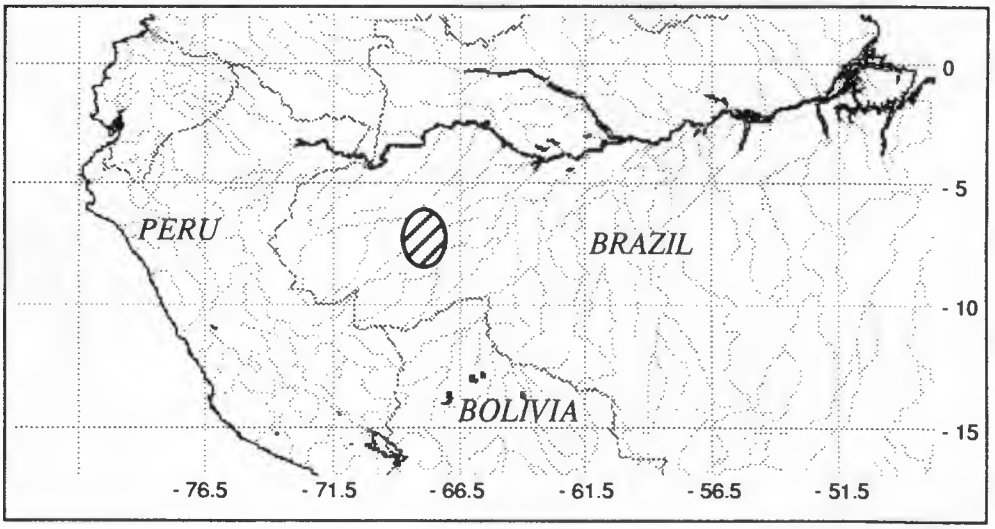

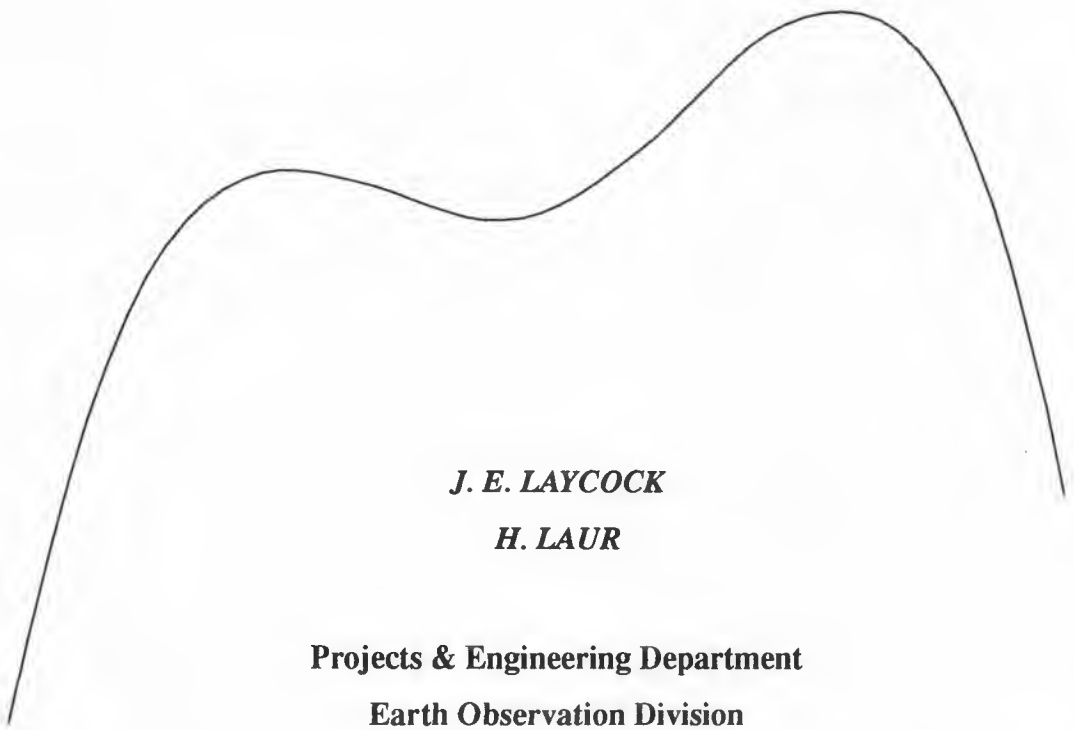

J. E. LAYCOCK

H. LAUR

Projects & Engineering Department

Earth Observation Division

ES-TN-DPE-OM-JL01, Issue 1, Rev. 1 ***September 1994***

Contents

			Page
1.0	Introduction		1
2.0	Method for Antenna Pattern Calculation		2
	2.1	Image Selection	3
	2.2	Antenna Pattern Extraction	3
	2.3	Key Assumptions	4
3.0	Results of Antenna Profile Estimation		5
4.0	VMP Application		7
	4.1	Accuracy of VMP Antenna Pattern Correction	7
	4.2	VMP Polynomial	7
5.0	Gamma Profile		9
6.0	Conclusions		10
Appendix A		The Improved Antenna Pattern	11
Appendix B		Converting SAR images to the New Pattern	13
Appendix C		Software	17
Figures			19

Acronyms and Abbreviations

ACS	Advanced Computer Systems
ADC	Analogue to Digital Convertor
MCS	Matra Cap Systemes
MPH	Main Product Header
PRI	ESA ERS Precision Image
SAR	Synthetic Aperture Radar
SARCALQ	ESRIN SAR Calibration and Quality Control System
SPH	Specific Product Header
VMP	Verification Mode Processor

ERS-1 SAR Antenna Pattern Estimation

J. E. Laycock, H. Laur

1.0 Introduction

This report covers:

- Re-estimation of the ERS-1 antenna pattern.
- Analysis of the way the VMP applies the antenna pattern.

The purpose of the antenna pattern re-estimation was to investigate reported anomalies [J. L. Valero, "Calibration and Validation of ERS-1, JERS-1 SAR", ESTEC ref XRI/037.94/JLV, March 1994] in the application of the current VMP antenna pattern, to derive an improved estimation of the SAR antenna pattern, and to establish a methodology (and software) for use in future.

The method used to derive the improved antenna pattern, together with some explanation of the approach adopted, is given in section 2, and the improved pattern is presented in section 3. Section 4 analyses the use of the antenna pattern data by the VMP, and analyses an anomaly in the way the pattern is currently applied. The γ profiles for the improved and original patterns are given in section 5, and conclusions are drawn in section 6.

A listing of the improved antenna pattern is given in Appendix A.

The scaling to be applied to images processed using the old pattern in order to achieve the same results as if the improved pattern was used, is given in Appendix B.

A brief description of the software used to derive the improved antenna pattern is given in Appendix C.

2.0 Method for Antenna Pattern Calculation

Homogeneous images over the Amazonian rainforest were selected, based on the assumption that $\gamma = \sigma^o/\cos\alpha$ is constant across such images. Processing such data without antenna pattern correction (but with range spreading loss correction applied) therefore means that the range amplitude variation of the resulting images represents the actual in flight antenna pattern.

In an ESA ERS SAR image, the average pixel intensity <I> can be related to the back-scattering coefficient σ^o by:

$$\sigma^o = \frac{\langle I \rangle}{K} \cdot \frac{\sin\alpha}{\sin\alpha_{REF}} \cdot \frac{R^3}{R^3_{REF}} \cdot \frac{1}{G^2(\theta)}$$

where α represents local incidence angle, θ represents look angle, R represents slant range distance, K is a calibration constant, and G represents the (one-way) antenna pattern [H. Laur, "Derivation of Backscattering Coefficient σ^o in ERS-1.SAR.PRI Products", ESRIN report dated 17th Oct. 1992]. Combining this with the expression for γ, ignoring constant terms and the range spreading loss (which is corrected independently) we get:

$$\gamma = \frac{I}{G^2(\theta)} \cdot \frac{\sin\alpha}{\cos\alpha}$$

This shows that in order to derive the antenna pattern intensity $G^2(\theta)$ from the image intensity <I> (as is the case here), it is necessary to divide by the cosine and multiply by the sine of the local incidence angle.

It should be noted that he ESA ERS SAR image intensity <I> is directly proportional to the radar brightness β^o [discussion from working groups 5 & 6, proc SAR Calibration Workshop, 1993], which is related to σ^o via:

$$\beta^o = \frac{\sigma^o}{\sin\alpha}$$

The method used to estimate the antenna pattern can be divided into two parts:

- Selection and processing of suitably homogeneous images
- Extraction of range profile and conversion to look-angle coordinates.

2.1 Image Selection

1. Two quick look images were generated using the MCS/ACS ("Bangkok") SAR processor. These correspond to a 3360km strip along orbit 4063 (25-APR-1992) and a 1530km strip along orbit 4793 (15-JUN-1992). The locations of these strips are shown in Figs 1 and 2. The quick-look data for orbit 4793 is illustrated in Fig 3, where it is presented in four sections.
2. PV-Wave analysis of the quick look images was used to select the best (i.e. most homogeneous) scenes for the antenna pattern analysis.
3. The selected scenes were then processed using the VMP. They were generated as standard PRI products but with the following changes:

   i) No antenna pattern correction

   ii) No slant range to ground range correction

   iii) Slant range pixel spacing of 5.0 metres
4. The selected scenes were then analysed using the quality assessment tool "Sarcalq" to check their suitability (i.e. their homogeneity), and to select the best parts of the images to be used for the antenna pattern derivation.

2.2 Antenna Pattern Extraction

The PV-Wave programs used to perform the antenna pattern extraction are described in Appendix B of this document.

5. The most homogeneous parts of the image (as determined by visual inspection) are averaged in azimuth in order to produce a single range profile, one value per slant range sample (i.e. approximately 7475 samples).
6. The raw data saturation correction is applied by subtracting decibel power values as determined in [G. Pacheco, "An assessment of the ERS-1 SAR ADC non-linearities", ESRIN internal report] from the decibel intensity values of the extracted antenna pattern profile.
7. The coordinates of the range profile are then transformed into angular offset relative to boresight, using geometry based on parameters extracted from the product annotations (SPH). Firstly, R_E, the Earth radius at the image centre is obtained from the centre scene latitude ϕ, using:

$$R_E^2 = \frac{(a^2 \cdot \cos\phi)^2 + (b^2 \cdot \sin\phi)^2}{(a \cdot \cos\phi)^2 + (b \cdot \sin\phi)^2}$$

where the semi-major and semi-minor axes are given by a=6378144m and b=6356759m. The antenna pattern for each angle θ from -3.5^o to $+3.5^o$ (in steps of 0.1^o) relative to the antenna boresight angle, which is assumed to be fixed at 20.35^o, is given by:

$$L = 20.35 + \theta$$

$$\alpha = \arcsin\{(H.\sin L) / R_E\}$$

$$\beta = \alpha - L$$

$$r = R_E . \sin \beta / \sin L$$

$$r_\theta = (r - R_0) / 5.0$$

where H is the distance of the satellite from the Earth centre, as computed using the central orbit state vector position, R_0 is the slant range distance to the first range pixel, and the range pixel spacing is 5.0 metres.

The value of r_θ then gives the sample number in the range antenna pattern corresponding to boresight offset angle θ. The 200 range profile samples centred on r_θ are then averaged in order to produce the antenna pattern value for offset angle θ. The value 200 was chosen experimentally, providing a good compromise between reducing the noise in the antenna profile without distorting its shape. Some of the values of r_θ will fall outside the range profile extent, and antenna pattern measurements for these boresight angle values cannot therefore be computed from the current image (but see the discussion in section 4.2). The output from this coordinate transformation is up to 71 amplitude samples in boresight angle coordinates.

8. Cosine and sine correction are then applied by multiplying each of the amplitude sample values by the square root of the tangent of the corresponding incidence angle α (as computed above).

9. Antenna patterns derived from different images are thus in a common coordinate system, and can be combined by averaging.

10. As a final step, the intensity data is converted to decibels, and referenced to zero at boresight. This zero-referencing has the effect only of a constant scaling factor applied uniformly across range, and does not affect the shape of the antenna pattern. It should, however, be taken into account when considering image calibration.

2.3 Key Assumptions

There are thus two key assumptions which are inherent in the way the antenna pattern has been estimated:

- Gamma remains constant across each of the rainforest images.
- The antenna boresight angle remains fixed at 20.35^o.

3.0 Results of Antenna Profile Estimation

Five images were selected from each of the quick look products (much of the quick look data was unsuitable).The properties of these images are summarised in the following tables.

For most of these images, the mean backscattering coefficient is approximately -7dB (corresponding to a mean amplitude of 370). It should however be noted that scenes 3, 4 and 5 from orbit 4793 have a much lower mean than normal. The reason for this is at present unclear.

Table 1: Orbit 4063 (25-APR-1992)

Scene No.	Time	Quality	Image mean	Scene centre lat/long
1	14:47:05.681	Good	369	-7.08, 291.85
2	14:45:28.713	Poor	376	-1.34, 293.15
3	14:47:24.885	Medium	374	-8.219, 291.59
4	14:48:00.002	Medium	378	-10.30, 291.10
5	14:48:26.674	Poor	377	-11.87, 290.73

Table 2: Orbit 4793 (15-JUN-1992)

Scene No.	Time	Quality	Image Mean	Scene centre lat/long
1	14:42:43.934	Medium	353	-1.04, 293.92
2	14:43:24.259	Poor	362	-3.43, 293.38
3	14:44:08.422	Good	248	-6.05, 292.80
4	14:44:23.784	Good	251	-6.95, 292.59
5	14:44:39.145	Good	252	-7.87, 292.38

Of these 10 images, Sarcalq analysis showed that scene 2 from each orbit was insufficiently homogeneous, and hence these scenes were not analysed further. By way of illustration, Fig 4 shows scene 4 from orbit 4793. Note the river across the middle of the image, which needed to be masked out when deriving the antenna pattern.

Fig 5 shows range profiles from scenes 3, 4 and 5 from orbit 4793. The profiles match each other very closely, which suggests that they represent a good approximation to the actual antenna pattern. The pattern obtained from these three images combined is shown in Fig. 6 (dotted line), with the current VMP antenna pattern [H. Laur, "Derivation of Backscattering Coefficient σ^o in ERS-1.SAR.PRI Products", ESRIN report dated 17th Oct. 1992] represented by the solid line.

Fig. 7 shows the four profiles from orbit 4063 and the profile from scene 1 of orbit

4793. The somewhat lumpy appearance of most of these curves confirms the Sarcalq inspection of these scenes, which shows them to have some structure which will interfere with the antenna pattern extraction. Only scene 1 from orbit 4063 appears sufficiently homogeneous. Using this one image to produce another antenna profile, we obtain the graph in Fig 8, which is very similar to Fig 6.

Fig 9 shows the four individual antenna patterns which would be obtained from each of the four best images, superimposed.

The stability of the antenna pattern over a period of time was tested using two scenes from the same area spanned by scenes 3 to 5 from orbit 4793 (see table 2), but acquired in November 1993. The resulting antenna pattern, shown in Fig 10, is close to the ones in Figs 6 and 8. Details of the images are given in Table 3. Note that the image means are closer to what would usually be expected.

Table 3: Orbit 12308 (22-NOV-1993)

Scene No.	Time	Quality	Image Mean	Scene centre lat/long
1	14:44:08.498	Medium	350	-6.37, 292.72
2	14:44:23.588	Medium	347	-7.27, 292.52

The positions of the best four images (i.e. scenes 3, 4 and 5 from orbit 4793 and scene 1 from orbit 4063) are shown in Fig. 11. Using these to derive an improved antenna pattern gives the result shown in Figure 12. As well as the current (in-flight) antenna pattern, this graph also shows the pre-flight antenna pattern, for comparison.

The ADC power loss for the four included images is shown in Fig. 13. The three curves corresponding to the orbit 4793 images are very similar; the dotted line represents the image used from orbit 4063.

4.0 VMP Application

The input antenna pattern is two-way, in intensity and expressed in decibels. The VMP fits a fourth order polynomial function of slant range time to this data, with the origin at an arbitrary offset (usually 847000 metres, approximately corresponding to mid-range) as given in the product annotations (SPH). This polynomial is used to calculate the antenna profile correction vector across the full range extent of the image. The vector is then converted to amplitude before being applied to every line of range-compressed data during processing.

4.1 Accuracy of VMP Antenna Pattern Correction

Some experiments were performed, processing scene 1 from orbit 4063 on the Alpha implementation (version 5) of the VMP using various antenna pattern files, and analysing the residual range profiles of the resulting images. The residual range profiles were computed by averaging the "best" (i.e. most homogeneous) section of 4000 range lines from each processed image.

Fig 14 shows the results of using the improved antenna pattern (with cosine and sine scaling and raw data saturation correction excluded). The upper curve shows the range profile without correction, and the lower curve shows the residual profile with antenna pattern correction applied (the vertical displacement has been introduced artificially to facilitate the comparison). For this result, the pattern had been extended to span 7^{o} to make it comparable with the current antenna pattern. The resulting residual profile (the lower curve) ought to be flat (allowing for noise). The fact that there is clearly some undulation suggests that the antenna pattern has not been well applied.

These results led to the question as to whether the antenna pattern is correctly handled within the VMP itself.

4.2 VMP Polynomial

Fig 15 shows the current input antenna pattern as supplied to the VMP (71 samples). The dashed line represents the corresponding polynomial as given by the coefficients in the SPH. There is obviously a significant discrepancy between the two curves.

Nevertheless, it was confirmed by comparison with an independent polynomial fitting routine (the PV-WAVE utility "POLY_FIT") that this polynomial is, in fact, the best fourth order polynomial which could be fitted (as a function of slant range time) to the input pattern. Using a fifth order polynomial was found to give virtually no improvement.

Truncating the extent of the input antenna pattern, however, does give a significant improvement to the quality of fit, as shown by the dotted line in Fig 15, which represents the best fourth order polynomial fit to the central 55 samples of the input antenna pattern (i.e. spanning only 5.4^{o} around boresight).

A corresponding analysis using the improved antenna pattern is given in Fig 16. Again, there is a significant improvement in the quality of fit if fewer samples are taken. It should be noted that the discrepancy shown in this graph between the input pattern and the fitted polynomial accounts well for the shape of the measured residual range profile given in Fig 14.

These results show that if a wide antenna pattern (e.g. spanning 7^o as in the current case) is used, the problem of obtaining the best polynomial fit across the whole pattern (some of which will lie outside the range of the image being processed) means that a poorer fit is achieved across the central portion of the image.

There is, of course, a trade-off to be made between getting a good fit across most of the image, and of having less accurate antenna pattern correction at near and far swath, where the VMP antenna pattern polynomial is extrapolating outside the available data, and hence beginning to deviate from the true correction. This is illustrated in Fig 17, which shows (for the current antenna pattern) the error in the polynomial approximation, as a function of the degree to which the input antenna pattern has been truncated; the near cut corresponds to no truncation (i.e. all 71 samples used), and the furthest cut corresponds to only 51 samples being used. As expected, the central portion becomes flatter, at the expense of increasing errors at the edges (for clarity the graph has been truncated at -0.6dB).

The lower curve in Fig 18 gives the result of using the central 55 samples of the improved pattern (i.e. -2.7^o to $+2.7^o$ relative to boresight). Clearly the resulting residual range profile is much flatter than before (compare with Fig. 14), the only anomalies being at the extreme edges of the image.

5.0 Gamma Profile

The residual range profile (antenna pattern correction having been performed) can be converted to γ using the equations in section 2, i.e. converting to intensity, dividing by the cosine of the local incidence angle, and multiplying by the sine of the local incidence angle. For the current antenna pattern, as applied by the VMP, the result is shown in Fig 19. For the current length of 71 values, the result is similar to the γ profiles reported in [J. L. Valero, "Calibration and Validation of ERS-1, JERS-1 SAR", ESTEC ref XRI/037.94/JLV, March 1994]. When only 55 values are used, the graph becomes straighter, but still displays a slope of approximately 0.7dB. Note that for clarity, the two curves have been shifted.

The corresponding results using the improved antenna pattern are given in Fig. 20. Note that for clarity, the two curves have been shifted.

It should be noted, therefore, that in order to achieve a constant across-track γ profile (once sine calibration has been performed), an ESA ERS SAR image of a perfectly homogeneous area would vary in intensity (almost linearly) across track by approximately 1.5dB, the intensity being higher at near swath than at far swath.

6.0 Conclusions

The anomalies which have been reported concerning the antenna pattern correction applied by the VMP have been accounted for.

An improved antenna pattern has been derived, using carefully selected rainforest images, which appears to give better results. Approximately 5000km of quick-look rainforest data was scanned in order to choose the four most homogeneous scenes which were used to derive the pattern.

As well as using more homogeneous rainforest images, the main differences between the way the improved and the original patterns were derived are:

- Filtering was used to smooth the antenna profile, rather than a fourth order polynomial fit.
- The effects of raw data saturation were taken into account.

In addition, an anomaly in the way the antenna pattern is applied by the VMP was discovered. The width of the current input antenna pattern (spanning 7^{o}) degrades the quality of the polynomial fit applied by the VMP. For the VMP, a shorter pattern (e.g. spanning only 5.4^{o}) should be used. The actual length should be selected as a trade-off between maintaining good accuracy across the central part of the image, whilst not allowing the errors at near and far swath to be too large.

It is recommended that in future upgrades of the VMP, the polynomial approximation is not used. If instead, for example, linear interpolation of the input pattern was used, then the above trade-off would not have to be performed, and the correction actually applied by the processor would correspond much more closely to the input antenna pattern. It has been found that the error in the applied antenna pattern due to a linear interpolation would be less than 0.006dB in amplitude.

Software has been produced to enable the process of antenna pattern extraction to be carried out more easily in future. This is described in Appendix C.

Appendix A: The Improved Antenna Pattern

TABLE 4. Improved Antenna Pattern

Degrees (rel. to Boresight)	Power (dB)
-3.1	-1.420
-3.0	-1.245
-2.9	-1.067
-2.8	-0.901
-2.7	-0.746
-2.6	-0.605
-2.5	-0.478
-2.4	-0.365
-2.3	-0.269
-2.2	-0.186
-2.1	-0.116
-2.0	-0.064
-1.9	-0.022
-1.8	0.012
-1.7	0.036
-1.6	0.053
-1.5	0.066
-1.4	0.071
-1.3	0.071
-1.2	0.067
-1.1	0.060
-1.0	0.053
-0.9	0.045
-0.8	0.035
-0.7	0.023
-0.6	0.011
-0.5	0.001
-0.4	-0.009
-0.3	-0.013
-0.2	-0.013
-0.1	-0.009
0.0	0.000

Degrees (rel. to Boresight)	Power (dB)
0.1	0.015
0.2	0.033
0.3	0.056
0.4	0.081
0.5	0.107
0.6	0.133
0.7	0.165
0.8	0.197
0.9	0.231
1.0	0.264
1.1	0.294
1.2	0.317
1.3	0.335
1.4	0.348
1.5	0.356
1.6	0.358
1.7	0.354
1.8	0.343
1.9	0.322
2.0	0.291
2.1	0.249
2.2	0.188
2.3	0.112
2.4	0.023
2.5	-0.085
2.6	-0.209
2.7	-0.334
2.8	-0.485

Appendix B: Converting SAR images to the new pattern

This section gives tables for converting an image processed using the current antenna pattern to one which would have been obtained by applying the improved pattern.

Table 5 gives the correction (in terms of angle relative to boresight) to apply to a PRI image generated using the old antenna pattern to obtain a PRI which would be obtained by applying the new pattern. It assumes that the old and new patterns are applied correctly. Table 5 applies to PRI products created with a linear interpolation of the antenna pattern (i.e. UK-PAF PRI products).

TABLE 5. Conversion from current to improved pattern

Degrees (rel. to Boresight)	Power (dB)
-2.8	0.205
-2.7	0.201
-2.6	0.189
-2.5	0.172
-2.4	0.154
-2.3	0.136
-2.2	0.119
-2.1	0.102
-2.0	0.091
-1.9	0.082
-1.8	0.073
-1.7	0.065
-1.6	0.058
-1.5	0.051
-1.4	0.045
-1.3	0.042
-1.2	0.039
-1.1	0.036
-1.0	0.033
-0.9	0.029
-0.8	0.027
-0.7	0.027
-0.6	0.027
-0.5	0.026
-0.4	0.026
-0.3	0.024
-0.2	0.017
-0.1	0.011
0.0	0.001

Degrees (rel. to Boresight)	Power (dB)
0.1	-0.012
0.2	-0.027
0.3	-0.042
0.4	-0.059
0.5	-0.072
0.6	-0.085
0.7	-0.101
0.8	-0.118
0.9	-0.133
1.0	-0.149
1.1	-0.162
1.2	-0.169
1.3	-0.172
1.4	-0.174
1.5	-0.173
1.6	-0.171
1.7	-0.170
1.8	-0.168
1.9	-0.165
2.0	-0.162
2.1	-0.160
2.2	-0.152
2.3	-0.146
2.4	-0.143
2.5	-0.144
2.6	-0.151
2.7	-0.183
2.8	-0.214

The correction applies to the intensity (i.e. squared) data.

This correction table would need to be converted to range coordinates in order to be used. Such a conversion would vary from image to image, and would need to be calculated using the geometry parameters contained in the SPH.

Table 6 allows for the case when the old antenna pattern has been modified by the VMP fourth order polynomial approximation, as discussed in section 4. It assumes, however, that the new pattern has been correctly applied (i.e. does not allow for any polynomial approximation introduced when applying the new pattern). Table 6 applies to PRI products created with a polynomial interpolation (D-PAF and ESRIN).

TABLE 6. Conversion from current (VMP) to improved pattern

Degrees (rel. to Boresight)	Power (dB)
-2.8	0.151
-2.7	0.125
-2.6	0.099
-2.5	0.076
-2.4	0.057
-2.3	0.043
-2.2	0.033
-2.1	0.025
-2.0	0.027
-1.9	0.031
-1.8	0.035
-1.7	0.041
-1.6	0.049
-1.5	0.055
-1.4	0.062
-1.3	0.071
-1.2	0.079
-1.1	0.087
-1.0	0.092
-0.9	0.095
-0.8	0.098
-0.7	0.102
-0.6	0.104
-0.5	0.104
-0.4	0.103
-0.3	0.098
-0.2	0.087
-0.1	0.074
0.0	0.057

Degrees (rel. to Boresight)	Power (dB)
0.1	0.035
0.2	0.011
0.3	-0.015
0.4	-0.043
0.5	-0.069

Degrees (rel. to Boresight)	Power (dB)
0.6	-0.093
0.7	-0.123
0.8	-0.151
0.9	-0.179
1.0	-0.205
1.1	-0.228
1.2	-0.244
1.3	-0.255
1.4	-0.262
1.5	-0.265
1.6	-0.265
1.7	-0.263
1.8	-0.258
1.9	-0.248
2.0	-0.235
2.1	-0.218
2.2	-0.193
2.3	-0.165
2.4	-0.136
2.5	-0.104
2.6	-0.072
2.7	-0.059
2.8	-0.041

In principle, the error in the polynomial approximation will depend on satellite altitude, latitude, and slant range start time. It was found, however, that the maximum variation owing to these factors is less than 0.0004dB and hence can be ignored.

The corrections are shown graphically in Figs. 21 and 22.

Appendix C: Software

Four programs were written in PV-Wave to perform the antenna pattern extraction. They are described briefly in this appendix.

Currently they are held in PCSWS1::[LAYCOCK.RFOREST]

The user is expected to have created sub-directories [.R<ORB_ID>] as described below.

C1. RNGPAT

This program expects as input a standard VMP slant range image in MPH/SPH format, on an exabyte cassette.

The program allows the user to specify adjacent blocks of range lines, and for each block (which is averaged in azimuth, and the resulting profile displayed on the screen) to specify a section, in range, to be masked out, i.e. to be excluded from the final range profile calculation. The remaining portions of data are then averaged in azimuth to produce a range profile of the input image. This final range profile is also displayed graphically.

The outputs from the program are:

- a range profile (approximately 7475 samples) in amplitude (slant range coordinates) named [.R<ORB-ID>]RNGPAT_<SCENE-ID>.DAT
- a copy of the MPH and SPH headers in [.R<ORB-ID>]MPHSPH_<SCENE-ID>.DAT
- a short text file summarising the key SPH parameters as used in this analysis, together with some parameters characterising the extracted range profile, in [.R<ORB-ID>]TEXT_<SCENE-ID>.DAT.

<ORB-ID> is an orbit identifier, and <SCENE-ID> a scene identifier supplied by the user.

C2. BEAMPAT

This program takes as input [.R<ORB-ID>]RNGPAT_<SCENE-ID>.DAT and [.R<ORB-ID>]TEXT_<SCENE-ID>.DAT.

It prompts the user for the name of a raw data saturation correction file (currently this is expected to be 100 samples long, spanning exactly the slant range image, in power dB) which it applies to the data. It also performs cosine correction, before converting the resulting pattern from slant range coordinates into angle-relative-to-boresight coordinates. Filtering is performed to reduce the noise in the antenna pattern.

The output from this program is then an antenna pattern of 71 values, ranging from -3.5° to 3.5° in steps of 0.1°, called [.R<ORB-ID>]BEAMPAT_<SCENE-ID>.DAT. In general, some of the extreme values will be zero, where the image has not fully spanned the full 7°.

C3. COMBINE

This program takes antenna patterns as produced by BEAMPAT (the user is prompted for their orbit and scene identifiers), and combines them using averaging, to produce a definitive antenna pattern. The result is written to a file (named by the user) which has exactly the same format as the antenna pattern file currently used by the VMP. Antenna pattern values corresponding to boresight angles for which no measurements were obtained are set to zero.

The output pattern, which is in intensity, is expressed in decibels.

The resulting antenna pattern is displayed graphically. The current version of this program also reads the current antenna pattern file (the user is prompted for its name) and plots it on the same axes for comparison.

C4. COMPARE

This program takes any number of antenna patterns as produced by BEAMPAT (the user is prompted for their orbit and scene identifiers), and plots them on common axes, so that the user can assess their quality.

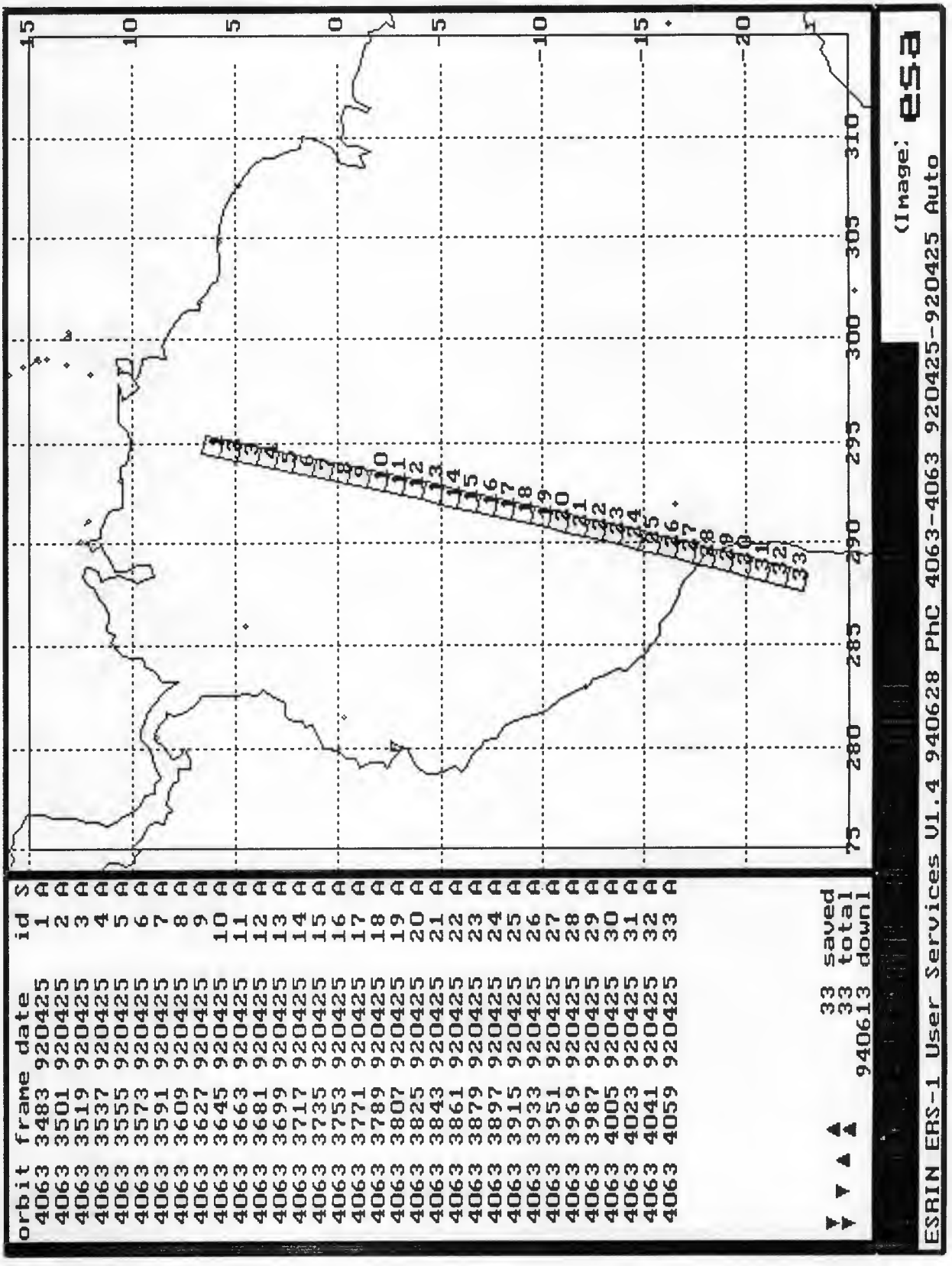

Fig 1 Quick-look location for Orbit 4063

Fig 2 Quick-look location for Orbit 4793

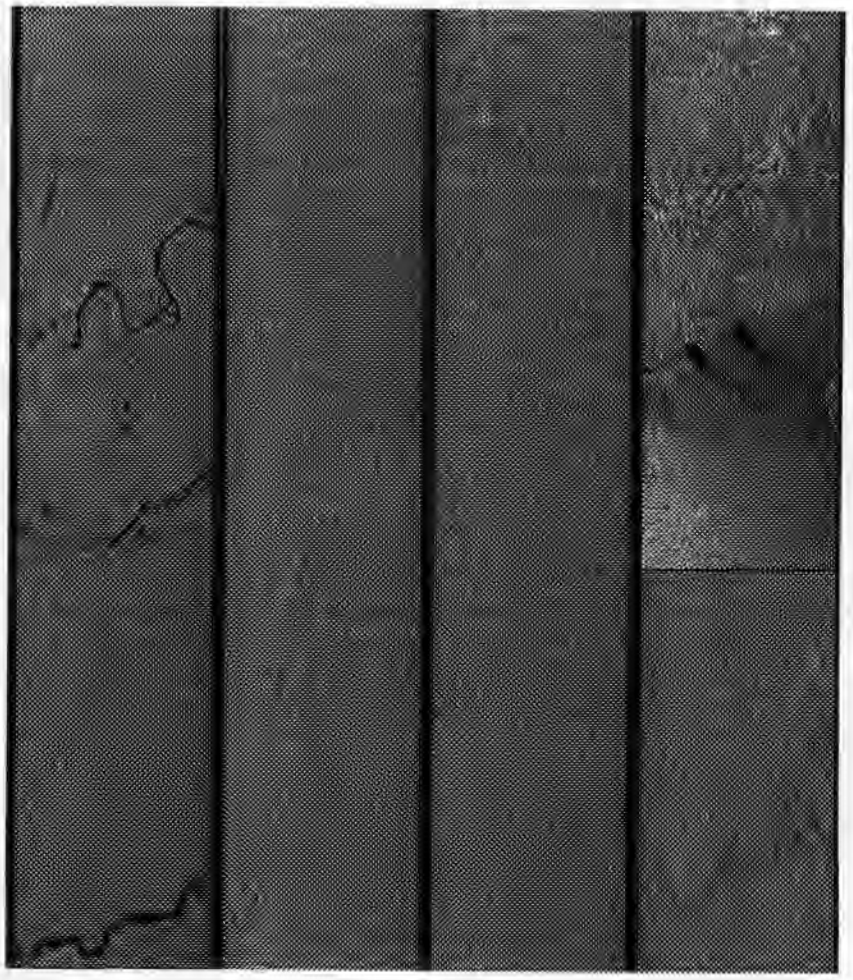

Fig 3 Quick-look of Orbit 4793

PRODUCT ID : 103455 (class 121) VI
ACQUISITION : 15-JUN-1992 14:44:23.784
GENERATION : 28-APR-1994 15:19:26.400
fourth rainforest image for antenna pattern analysis

(-7.52 , 292.96) (-7.32 , 292.12)
: corners
(-6.60 , 293.16) (-6.41 , 292.32)

NORTH VECTOR

Fig 4 Orbit 4793 Scene No. 4

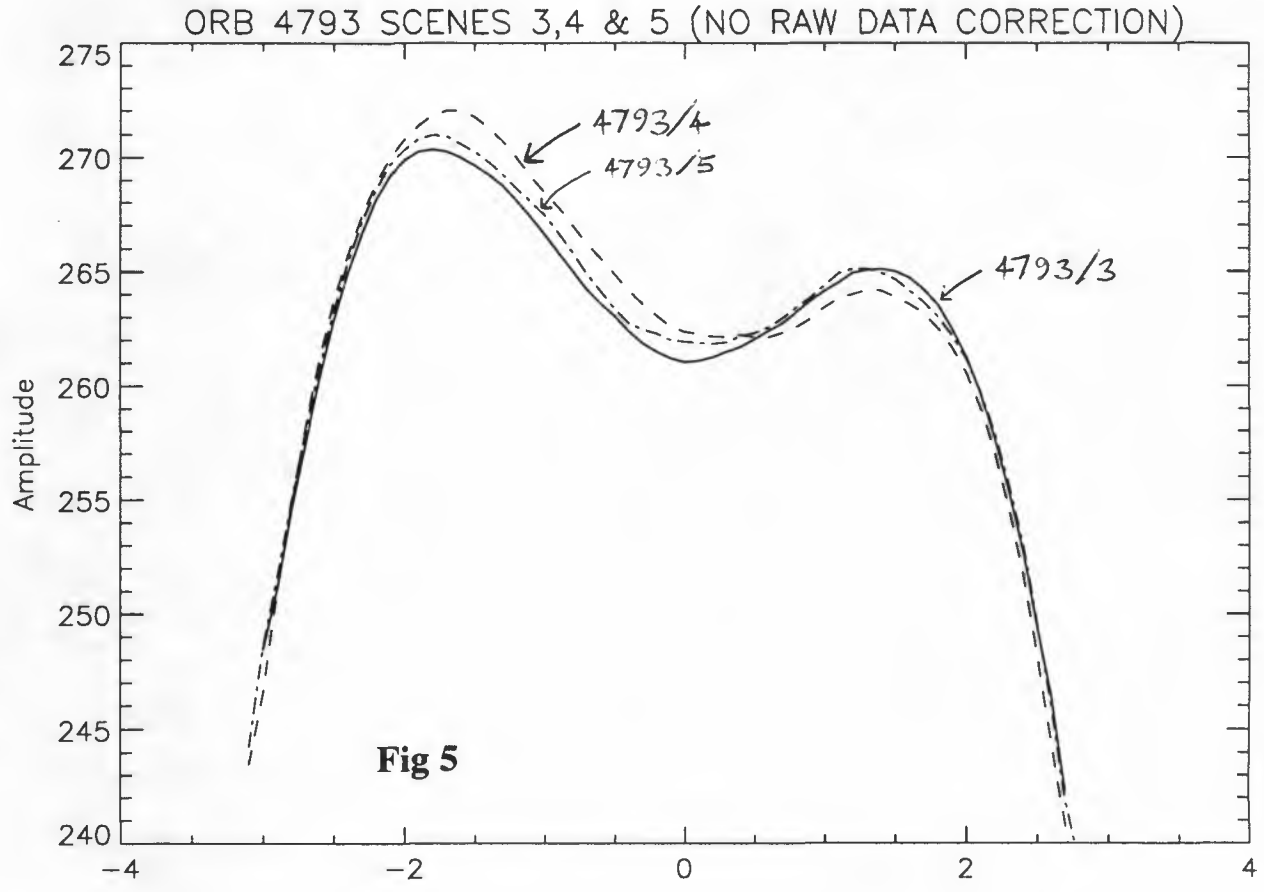
ORB 4793 SCENES 3,4 & 5 (NO RAW DATA CORRECTION)
Amplitude
275
270
265
260
255
250
245
240
−4
−2
0
2
4
4793/4
4793/5
4793/3

Fig 5

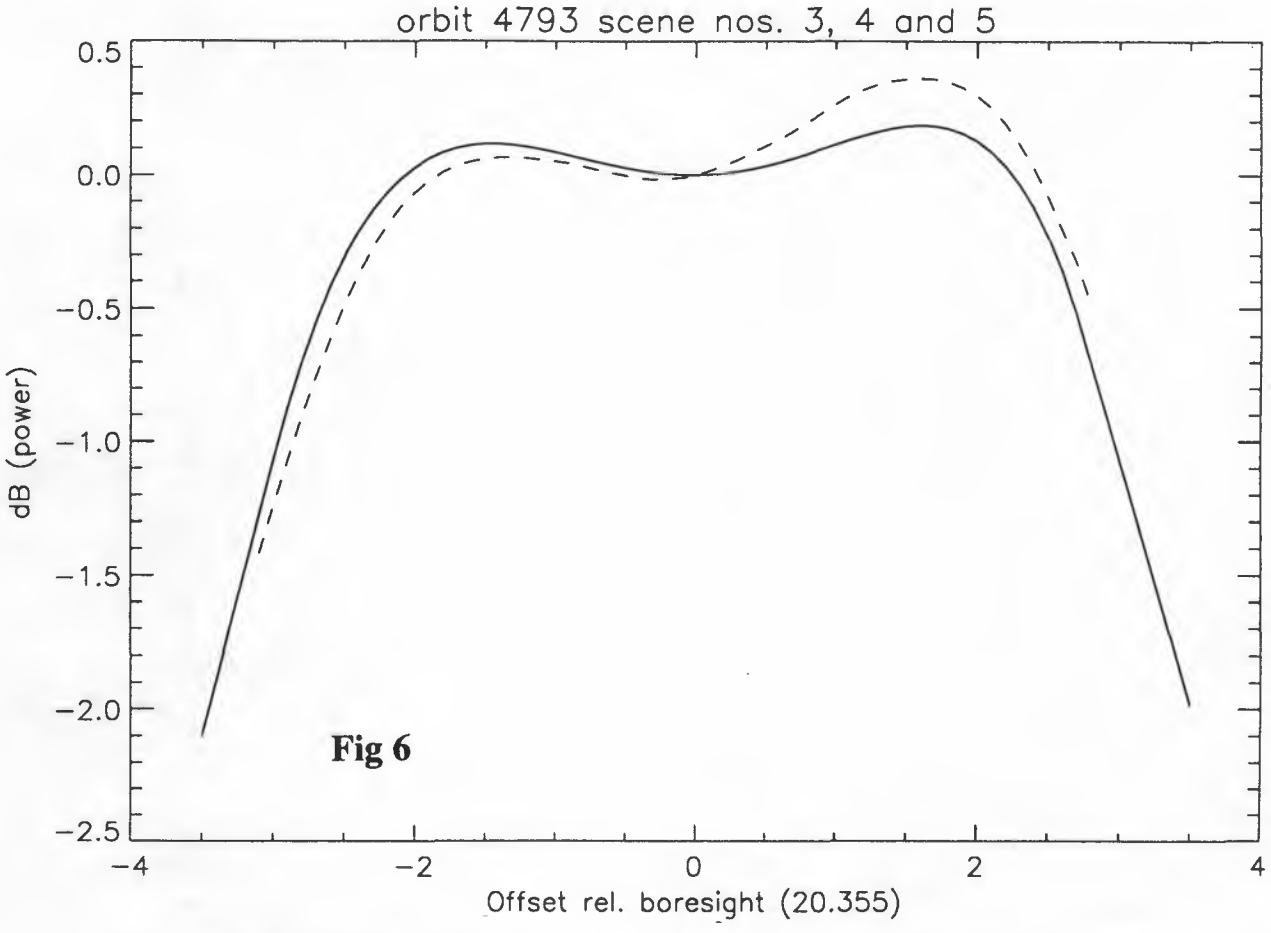
orbit 4793 scene nos. 3, 4 and 5
dB (power)
0.5
0.0
−0.5
−1.0
−1.5
−2.0
−2.5
−4
−2
0
2
4
Offset rel. boresight (20.355)

Fig 6

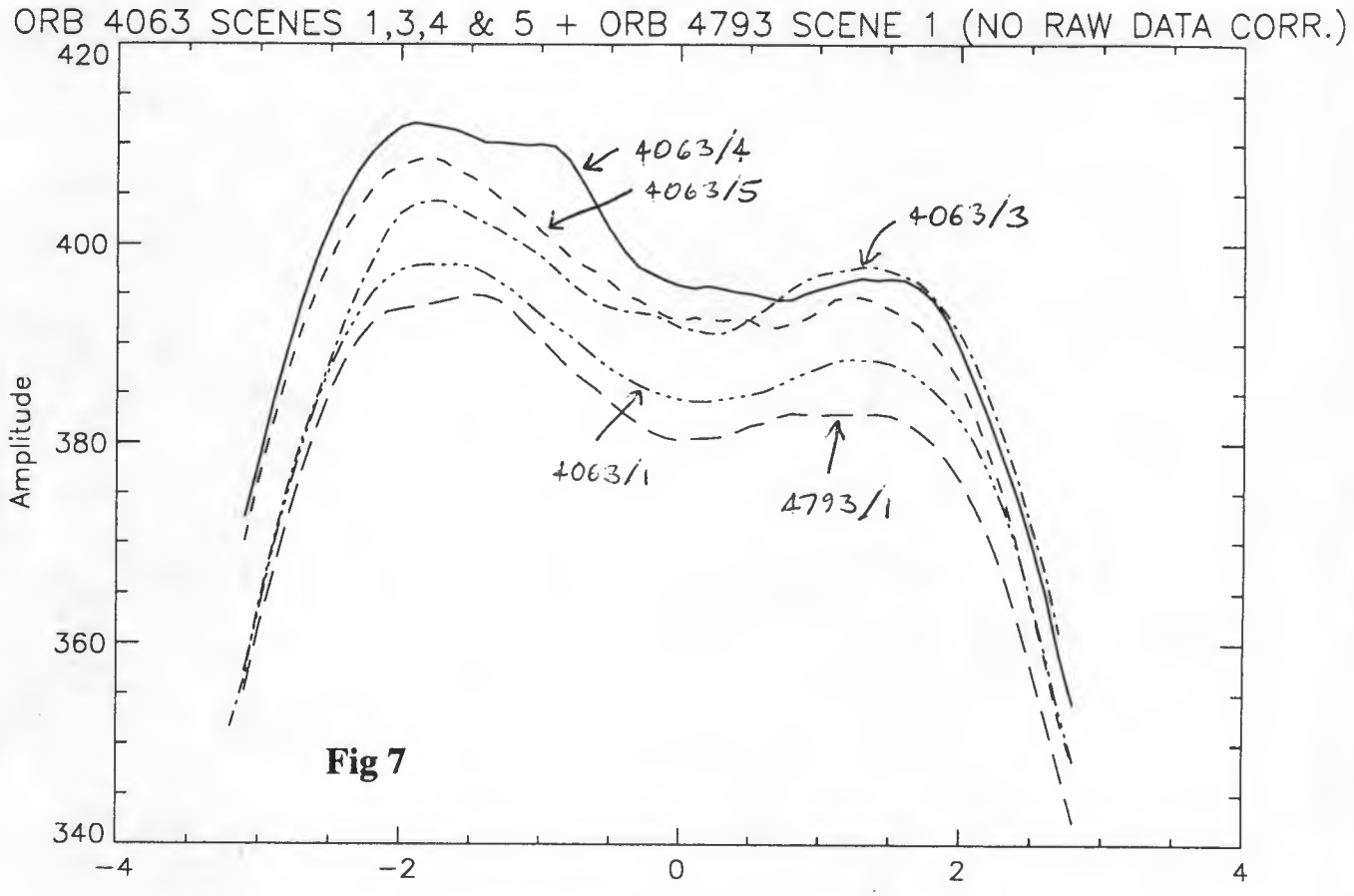
ORB 4063 SCENES 1,3,4 & 5 + ORB 4793 SCENE 1 (NO RAW DATA CORR.)
Amplitude
420
400
380
360
340
−4
−2
0
2
4
4063/4
4063/5
4063/3
4063/1
4793/1

Fig 7

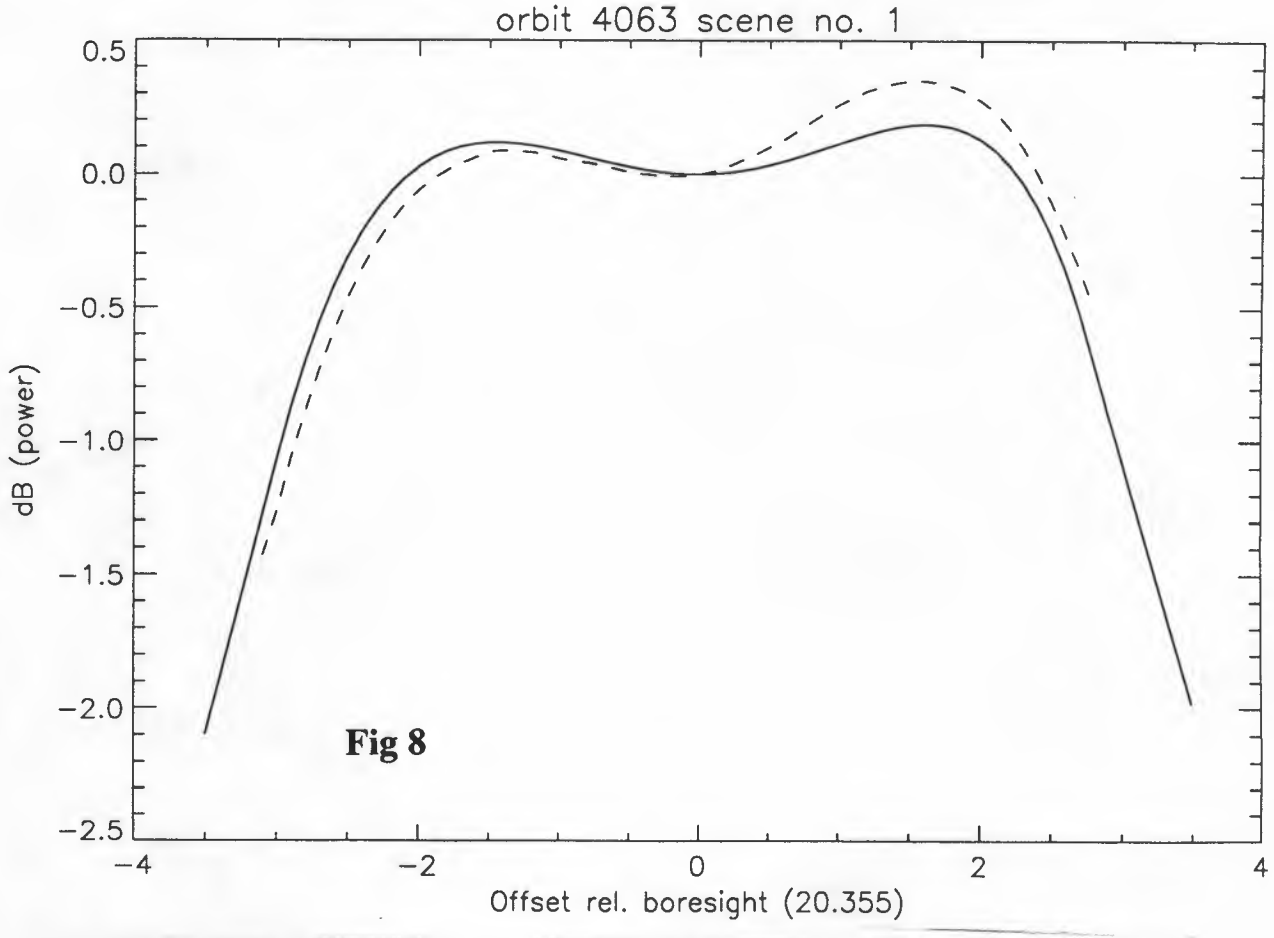
orbit 4063 scene no. 1
dB (power)
0.5
0.0
−0.5
−1.0
−1.5
−2.0
−2.5
−4
−2
0
2
4
Offset rel. boresight (20.355)

Fig 8

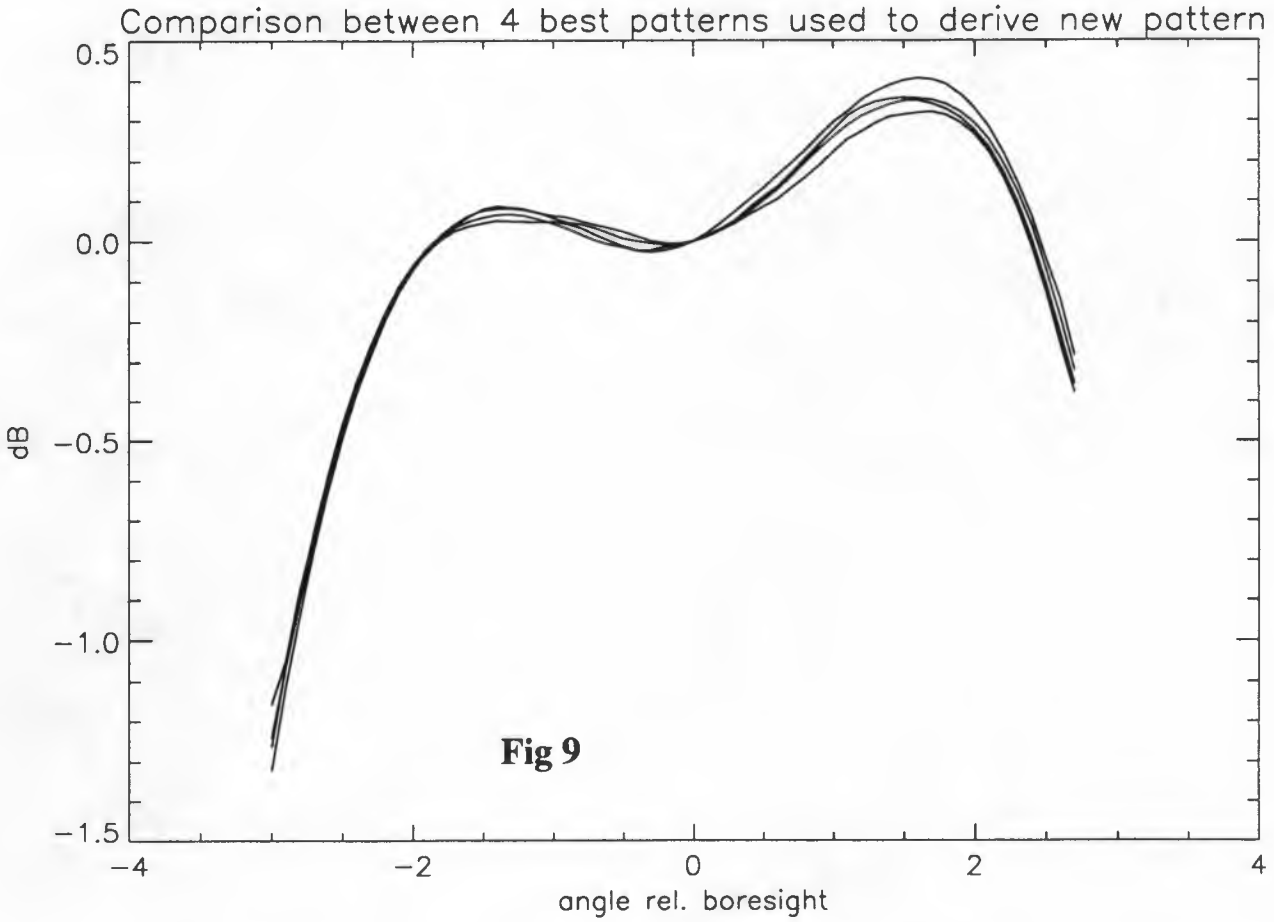
Comparison between 4 best patterns used to derive new pattern
0.5
0.0
−0.5
−1.0
−1.5
dB
−4
−2
0
2
4
angle rel. boresight

Fig 9

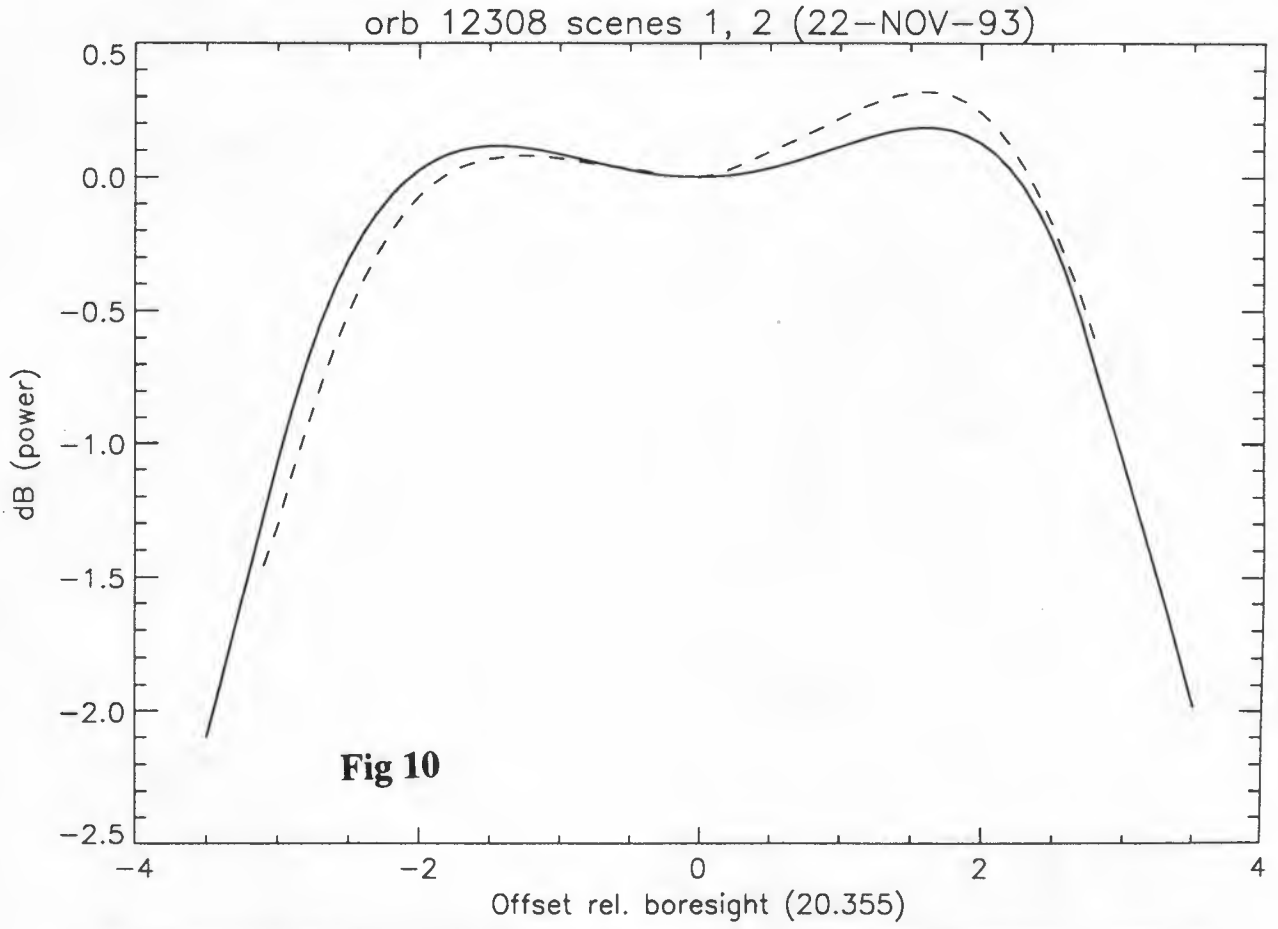
orb 12308 scenes 1, 2 (22−NOV−93)
0.5
0.0
−0.5
−1.0
−1.5
−2.0
−2.5
dB (power)
−4
−2
0
2
4
Offset rel. boresight (20.355)

Fig 10

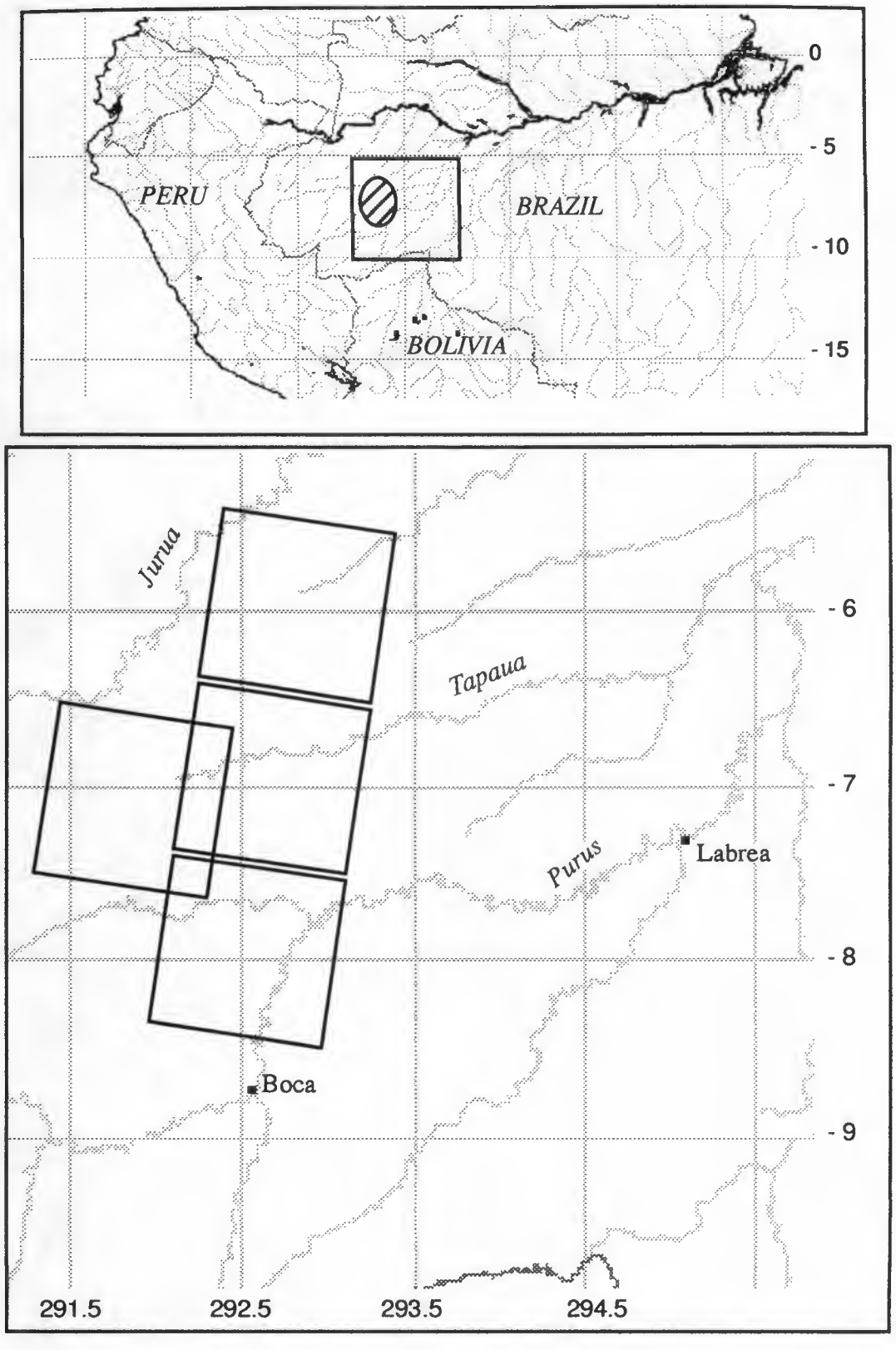

Fig 11 Location of the four selected scenes

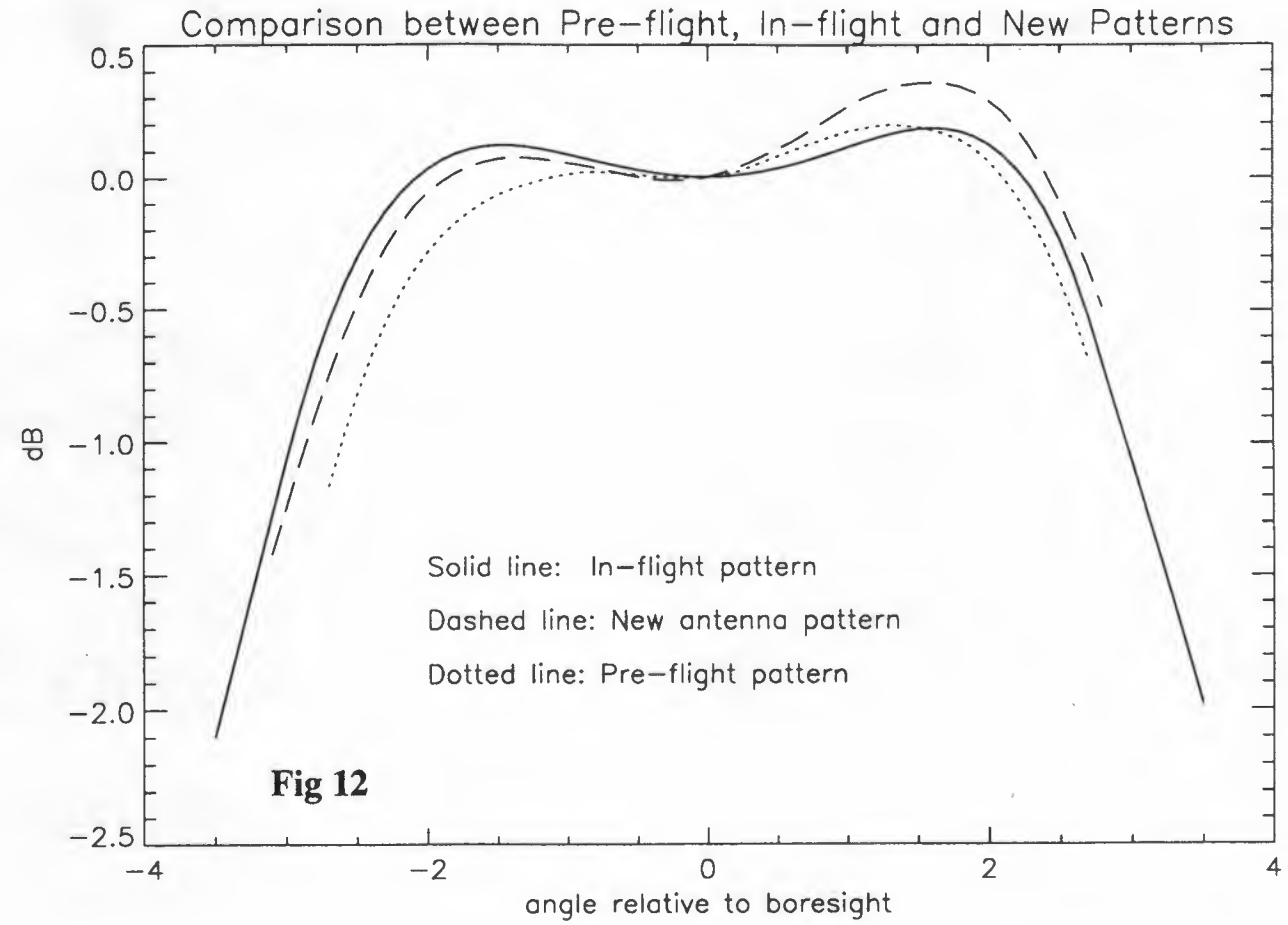
Comparison between Pre−flight, In−flight and New Patterns
0.5
0.0
−0.5
−1.0
−1.5
−2.0
−2.5
dB
−4
−2
0
2
4
angle relative to boresight
Solid line: In−flight pattern
Dashed line: New antenna pattern
Dotted line: Pre−flight pattern

Fig 12

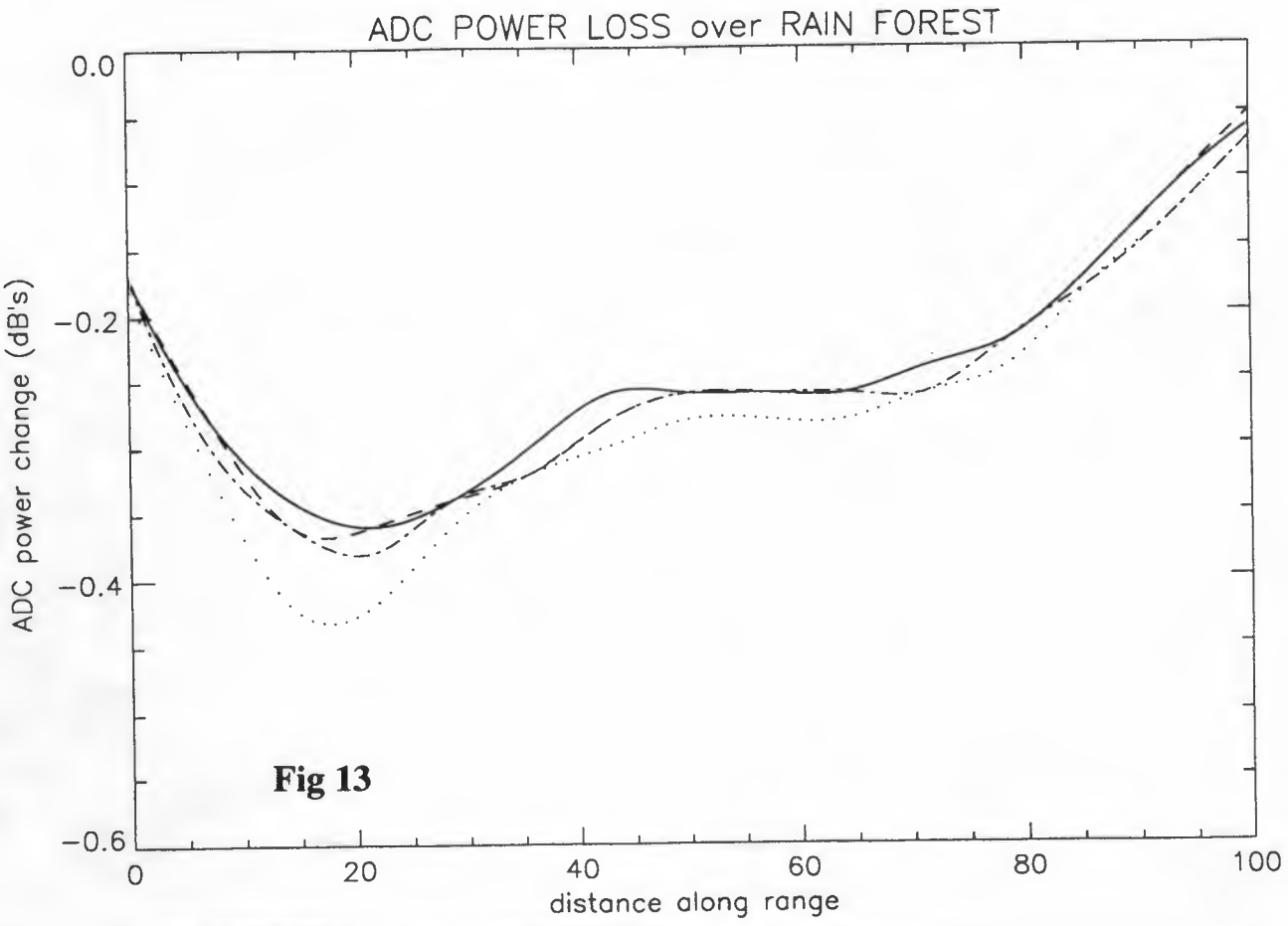
ADC POWER LOSS over RAIN FOREST
0.0
−0.2
−0.4
−0.6
ADC power change (dB's)
0
20
40
60
80
100
distance along range

Fig 13

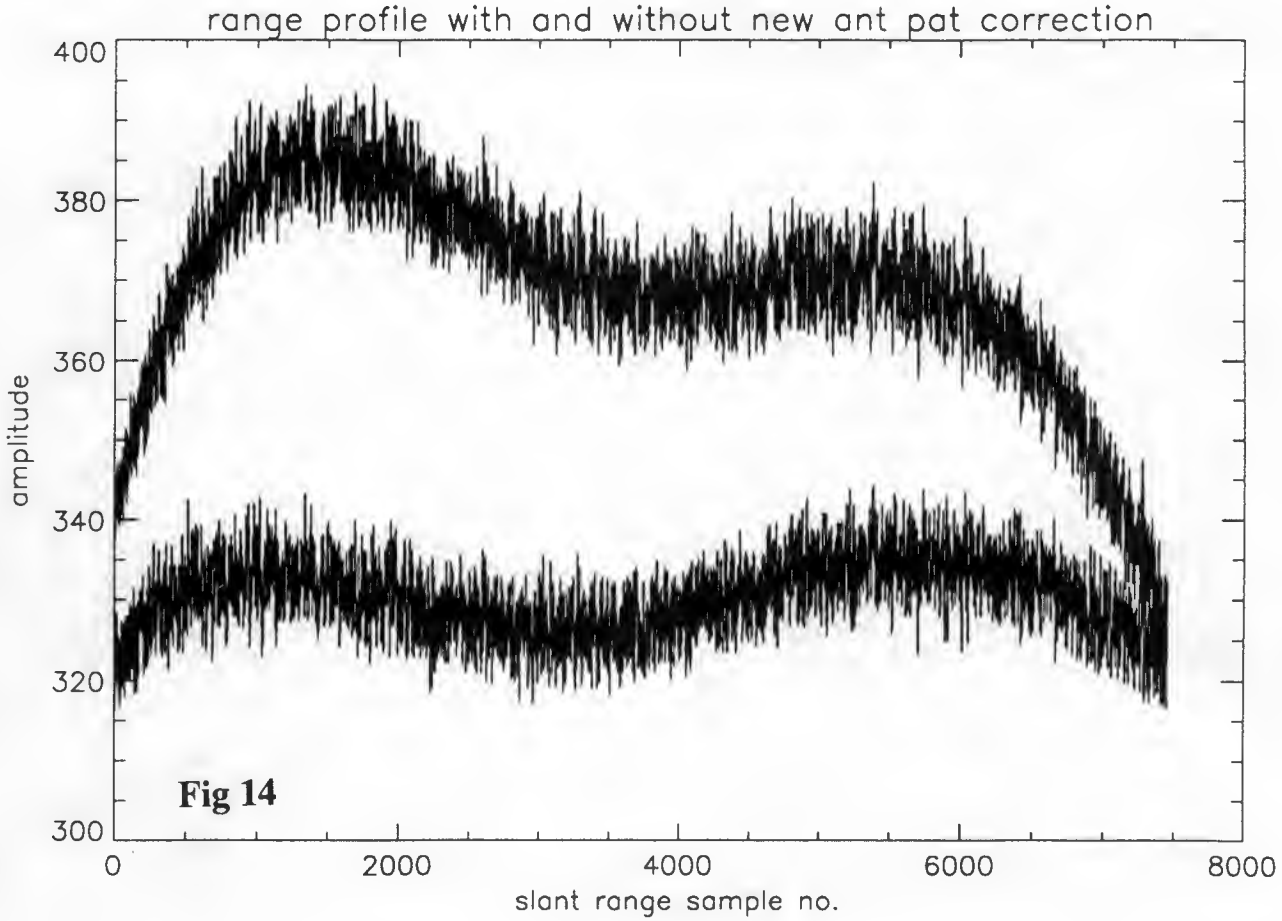
range profile with and without new ant pat correction
amplitude
400
380
360
340
320
300
0
2000
4000
6000
8000
slant range sample no.

Fig 14

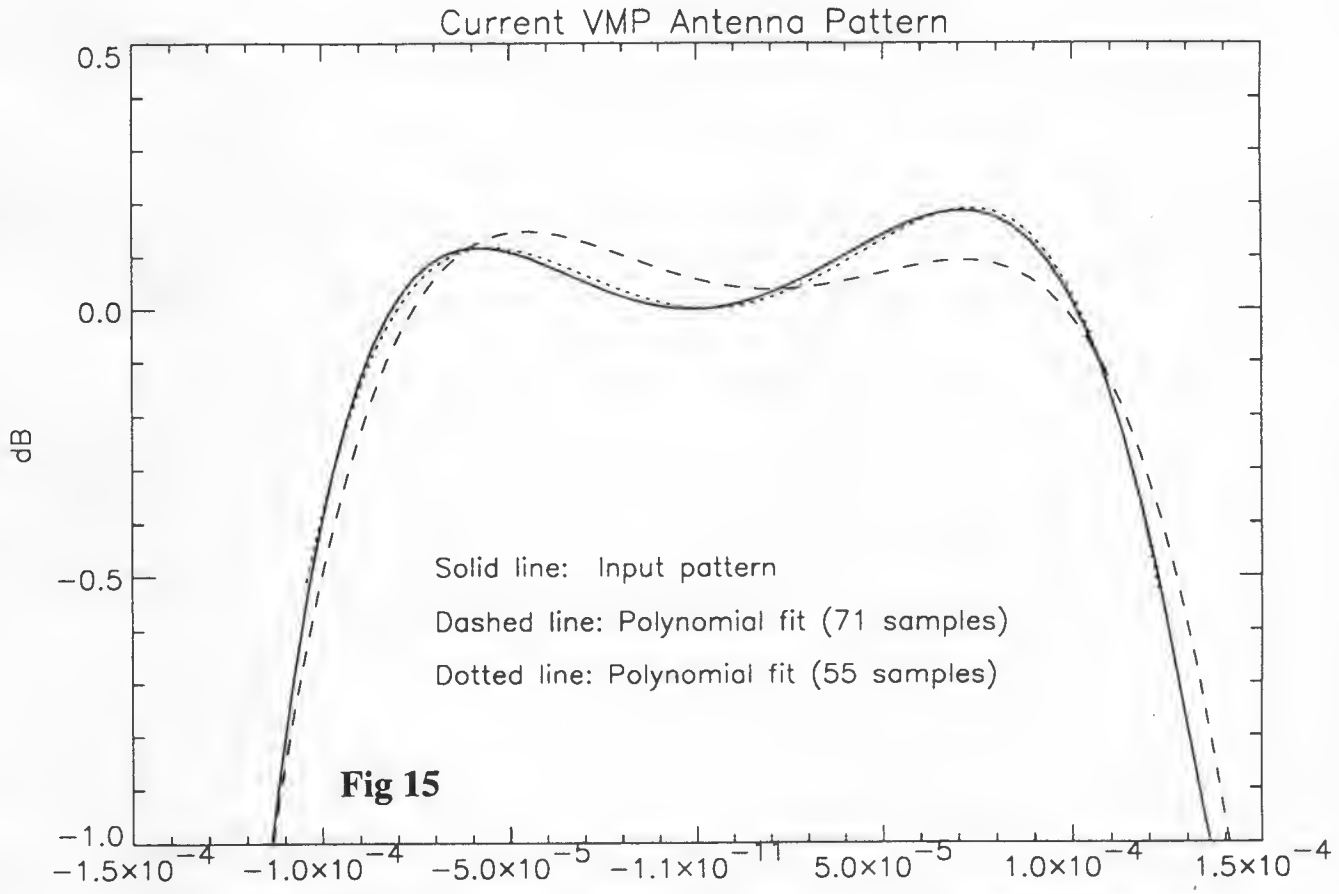
Current VMP Antenna Pattern
dB
0.5
0.0
−0.5
−1.0
−1.5×10^−4
−1.0×10^−4
−5.0×10^−5
−1.1×10^−11
5.0×10^−5
1.0×10^−4
1.5×10^−4
Solid line: Input pattern
Dashed line: Polynomial fit (71 samples)
Dotted line: Polynomial fit (55 samples)

Fig 15

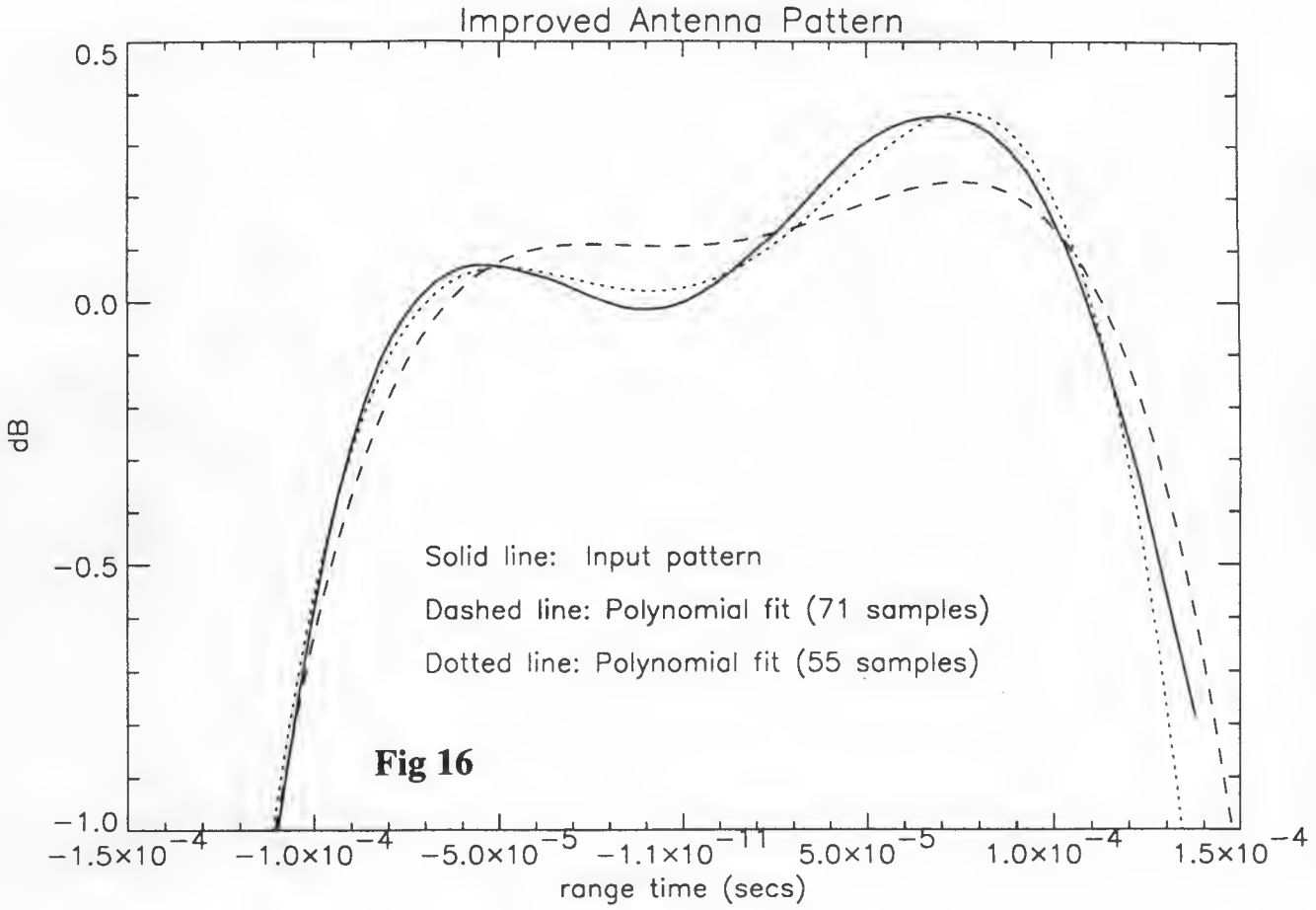

Fig 16

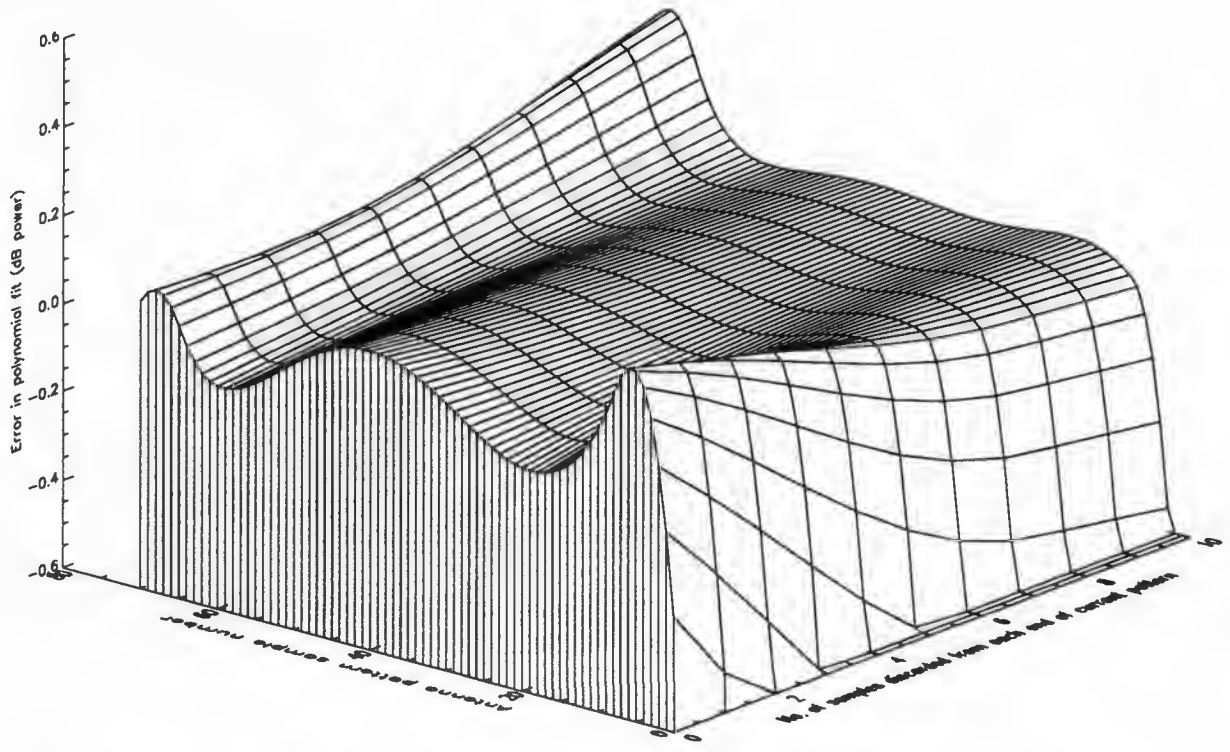

Fig 17 Poly Fit Error as a function of Input Length: Current Pattern

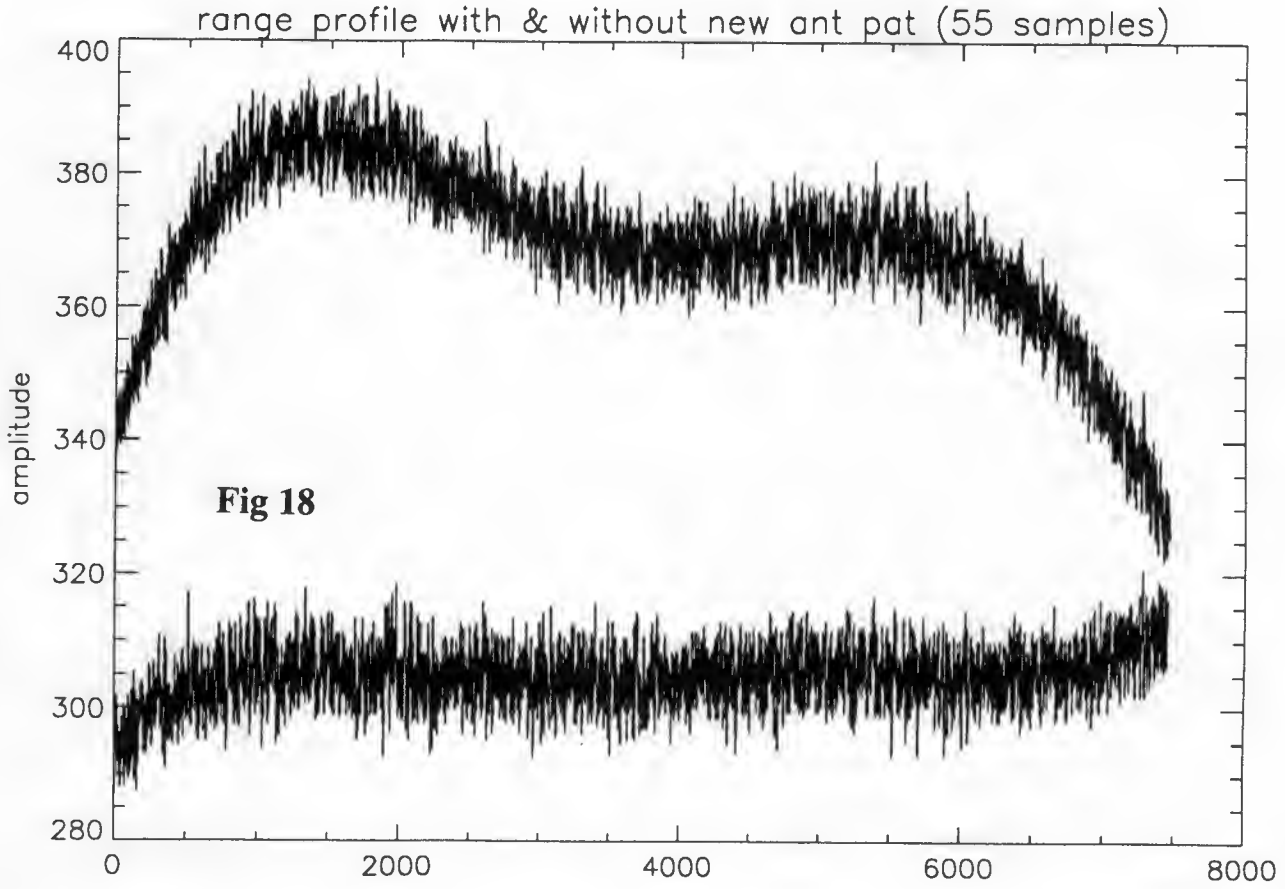

Fig 18

18

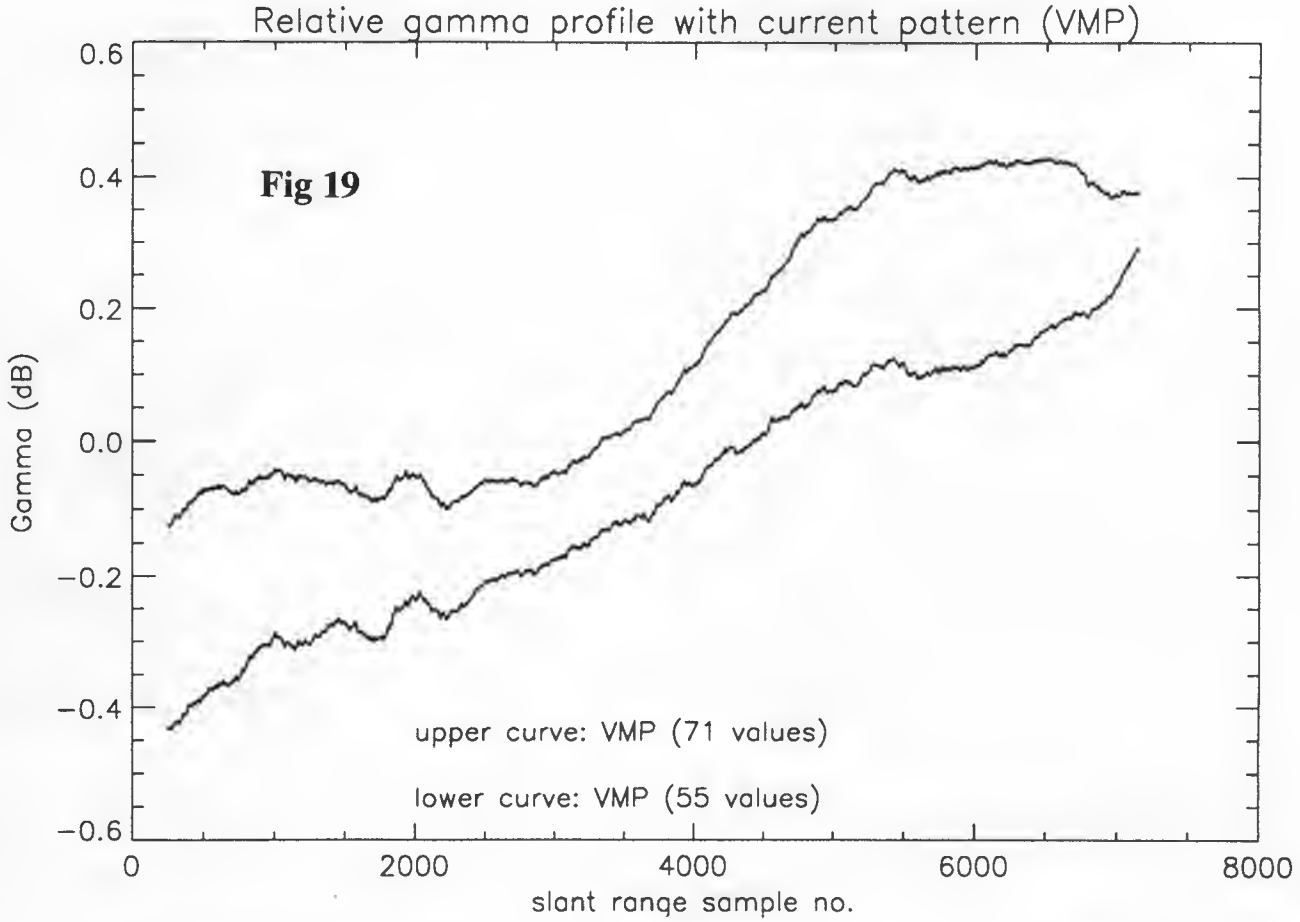

Fig 19

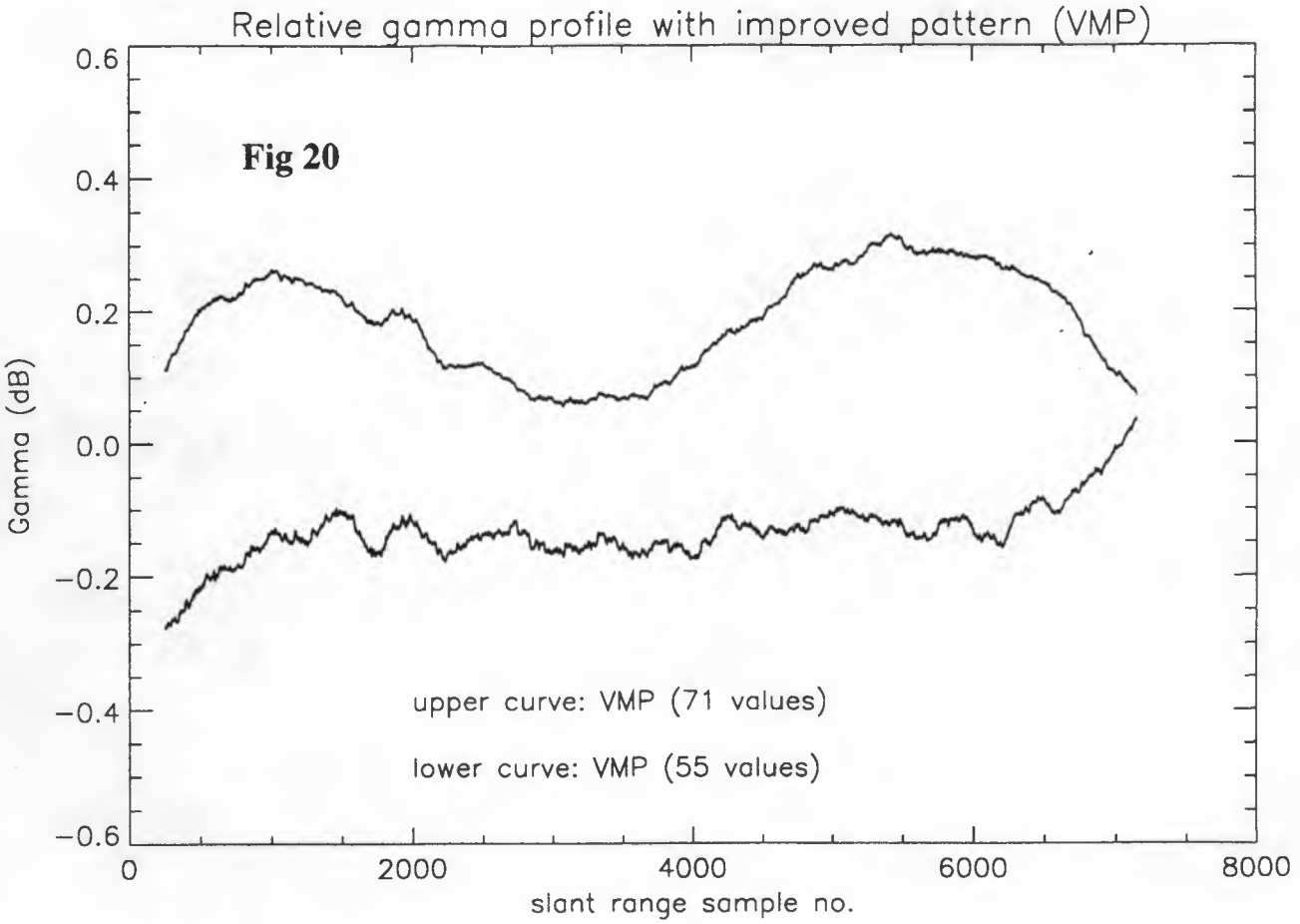
Relative gamma profile with improved pattern (VMP)
Fig 20
Gamma (dB)
0.6
0.4
0.2
0.0
−0.2
−0.4
−0.6
0
2000
4000
6000
8000
slant range sample no.
upper curve: VMP (71 values)
lower curve: VMP (55 values)

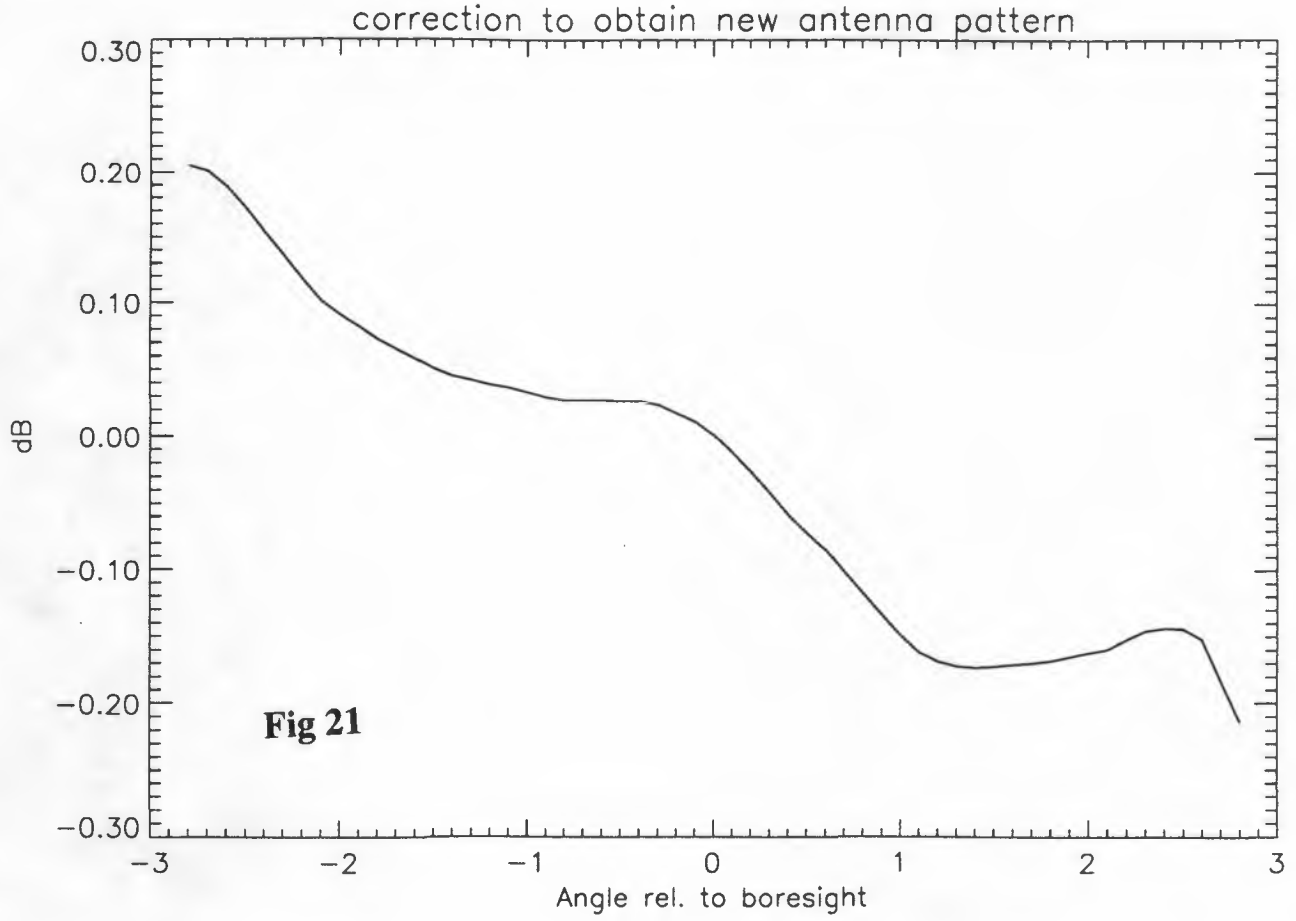
correction to obtain new antenna pattern
0.30
0.20
0.10
0.00
−0.10
−0.20
−0.30
dB
−3
−2
−1
0
1
2
3
Angle rel. to boresight

Fig 21

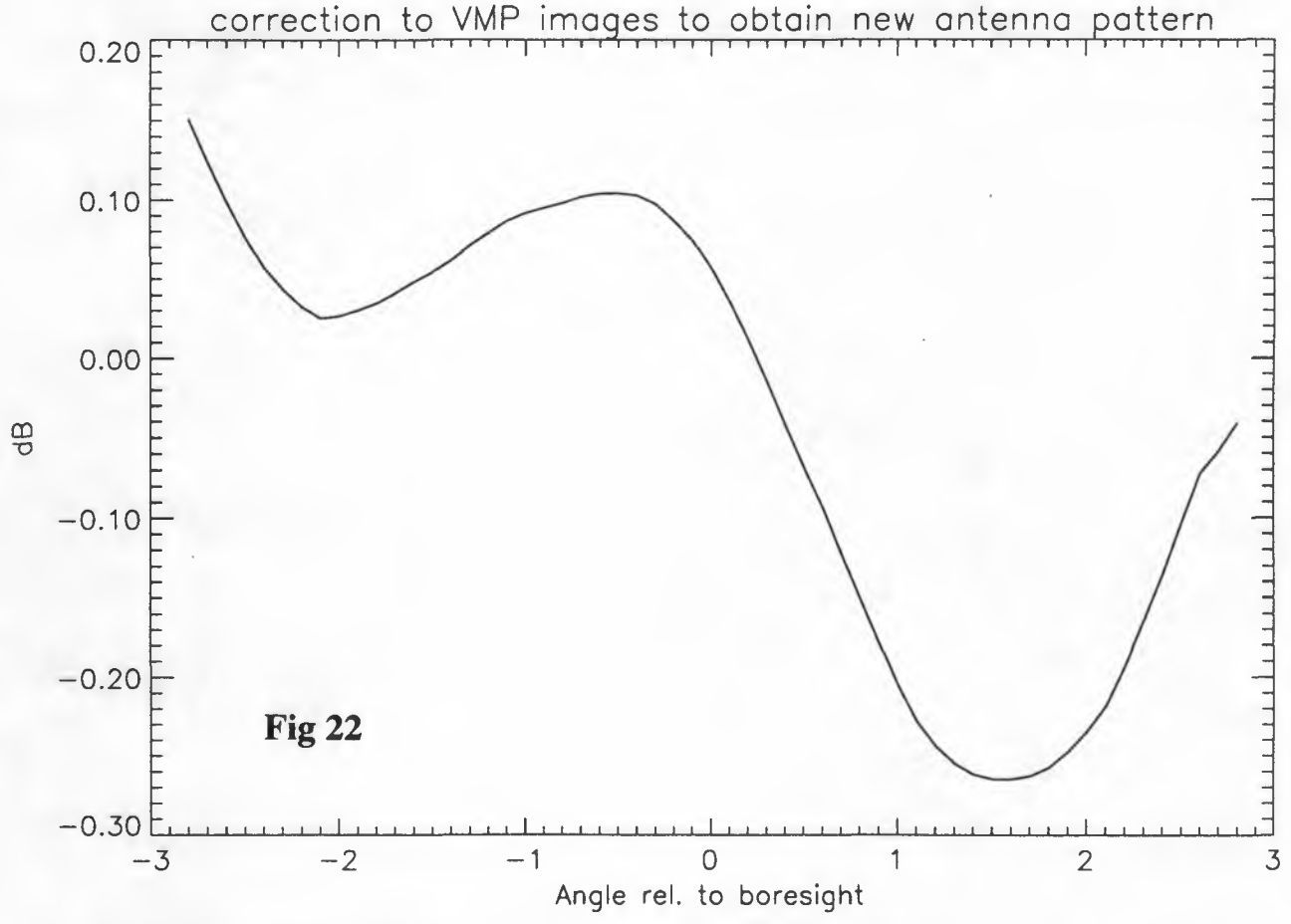
correction to VMP images to obtain new antenna pattern
0.20
0.10
0.00
−0.10
−0.20
−0.30
dB
−3
−2
−1
0
1
2
3
Angle rel. to boresight

Fig 22

esa esrin

european space agency
agence spatiale européenne

ERS-1 SAR Antenna Pattern Estimation

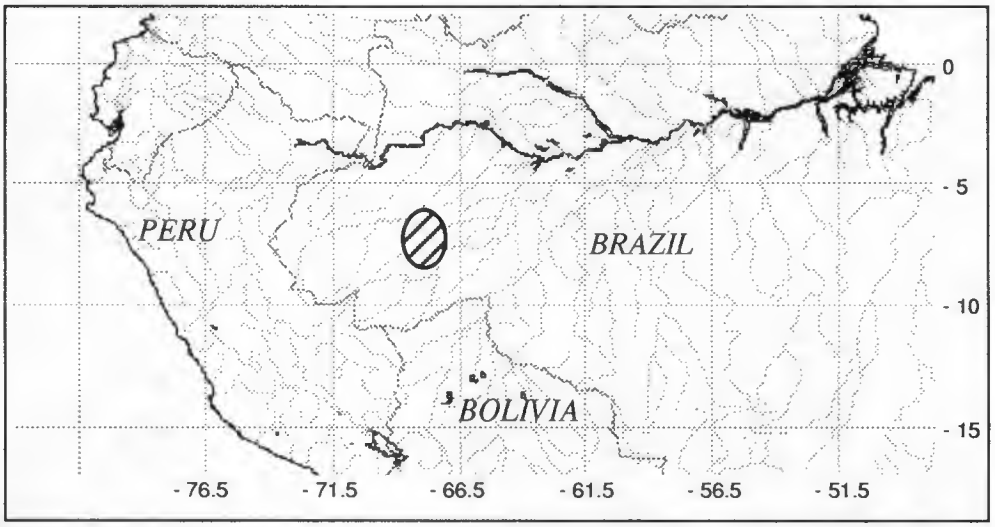

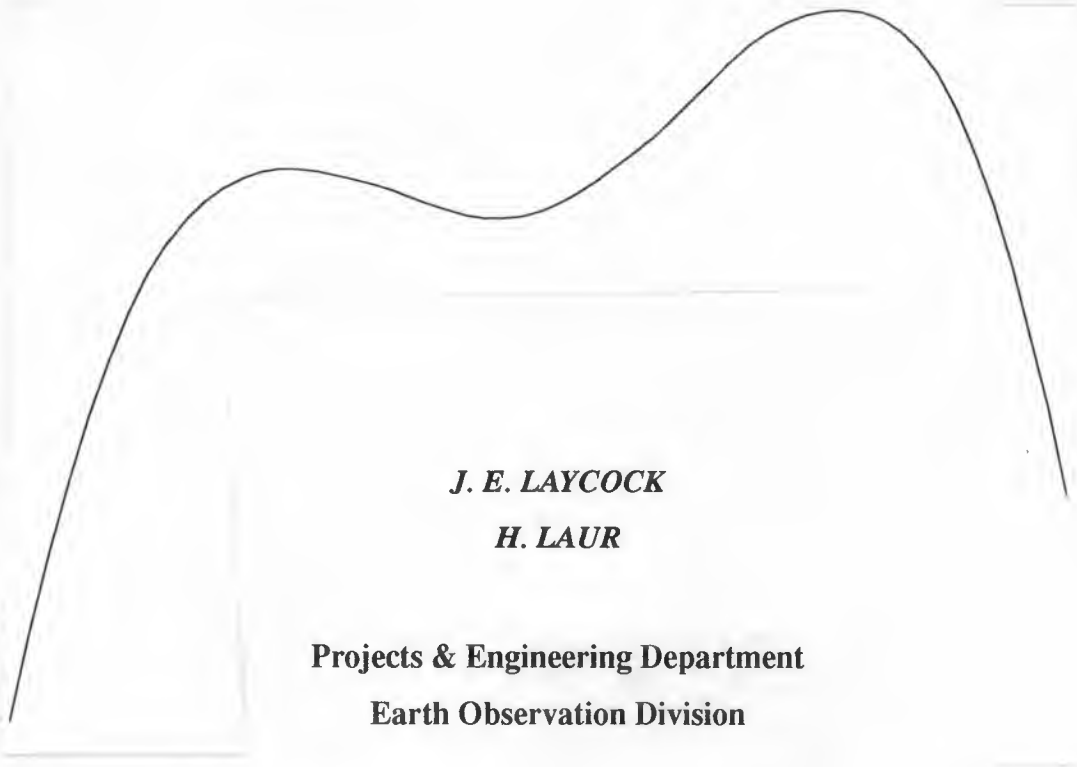

J. E. LAYCOCK

H. LAUR

Projects & Engineering Department

Earth Observation Division

ES-TN-DPE-OM-JL01, Issue 1, Rev. 1 *September 1994*

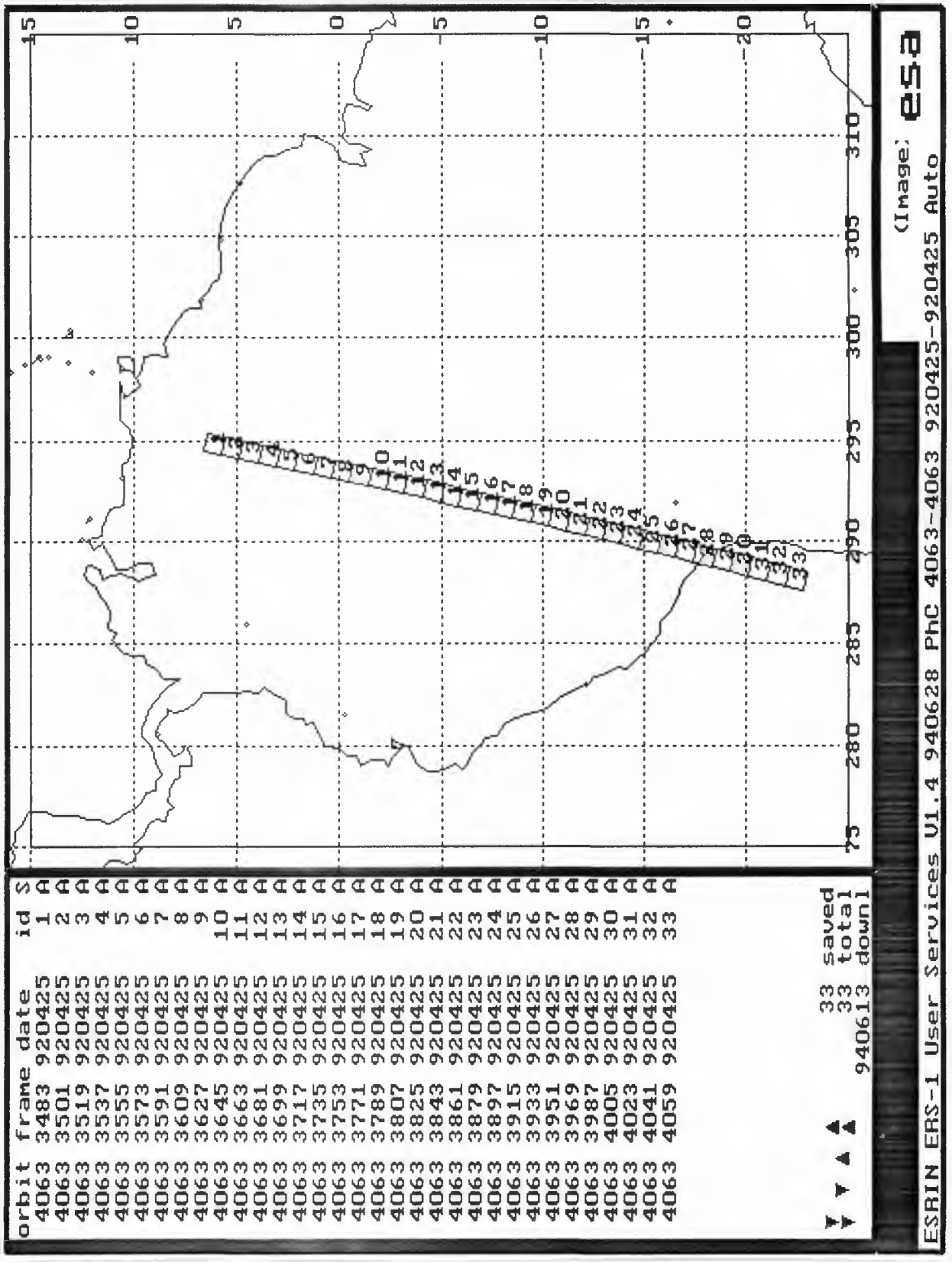

Fig 1 Quick-look location for Orbit 4063

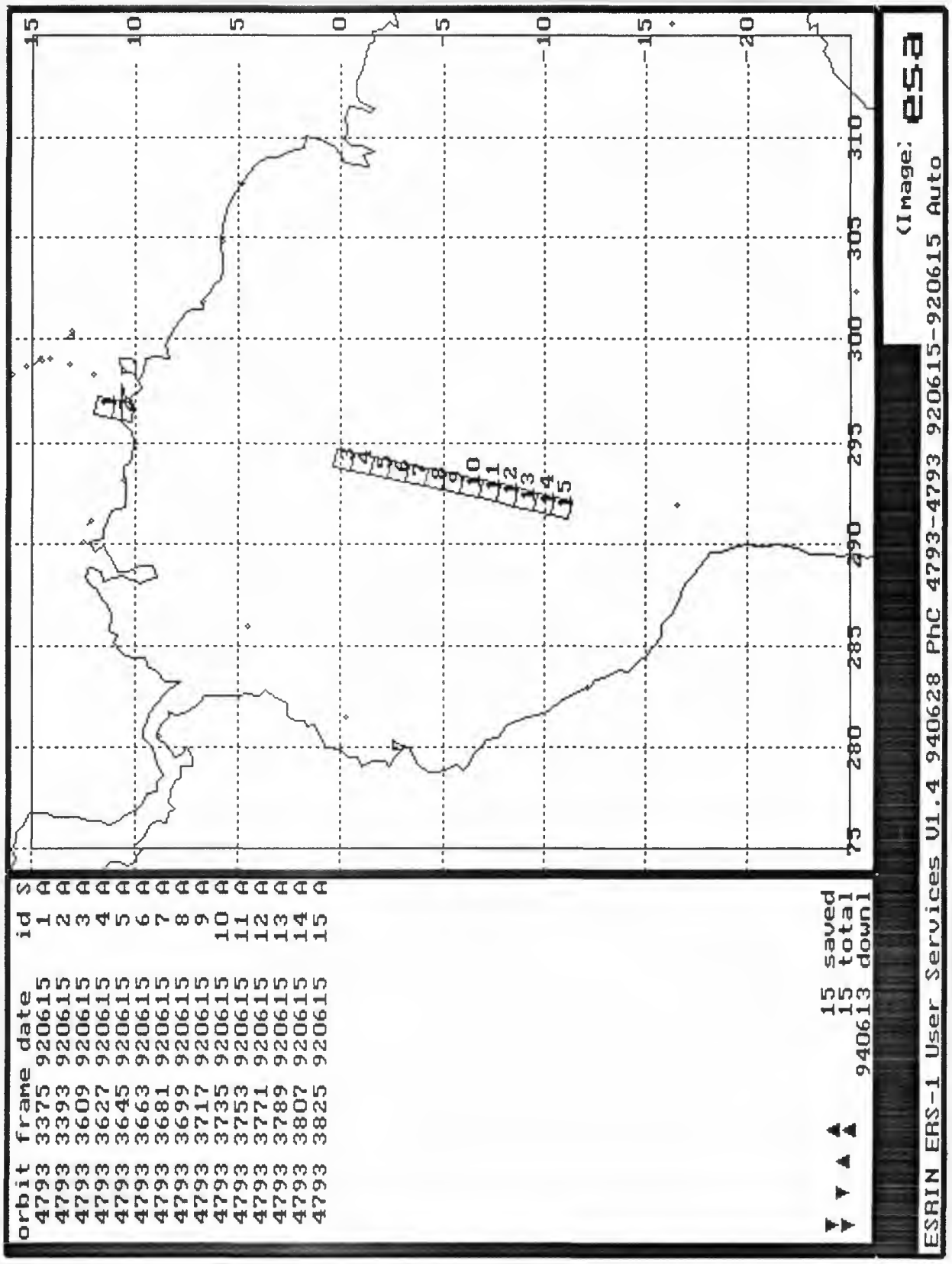

Fig 2 Quick-look location for Orbit 4793

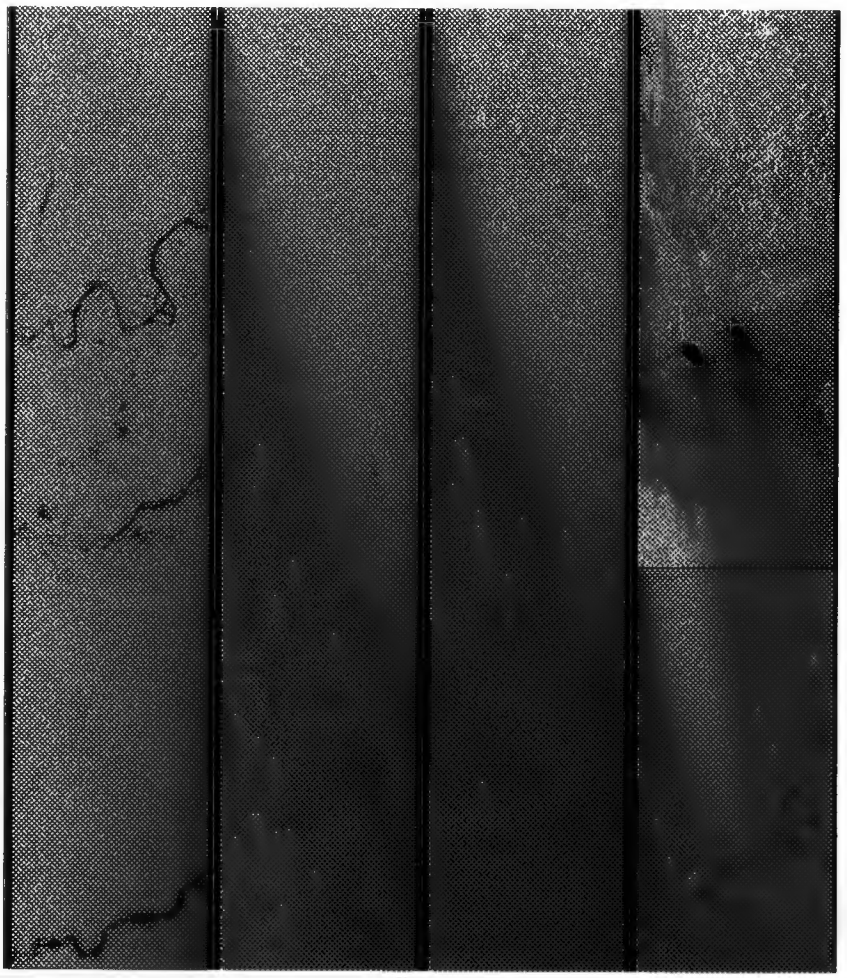

Fig 3 Quick-look of Orbit 4793

PRODUCT ID : 103455 (class 121) VI
ACQUISITION : 15-JUN-1992 14:44:23.784
GENERATION : 28-APR-1994 15:19:26.400
fourth rainforest image for antenna pattern analysis

(-7.52 , 292.96) (-7.32 , 292.12)
: corners
(-6.60 , 293.16) (-6.41 , 292.32)

NORTH VECTOR

Fig 4 Orbit 4793 Scene No. 4

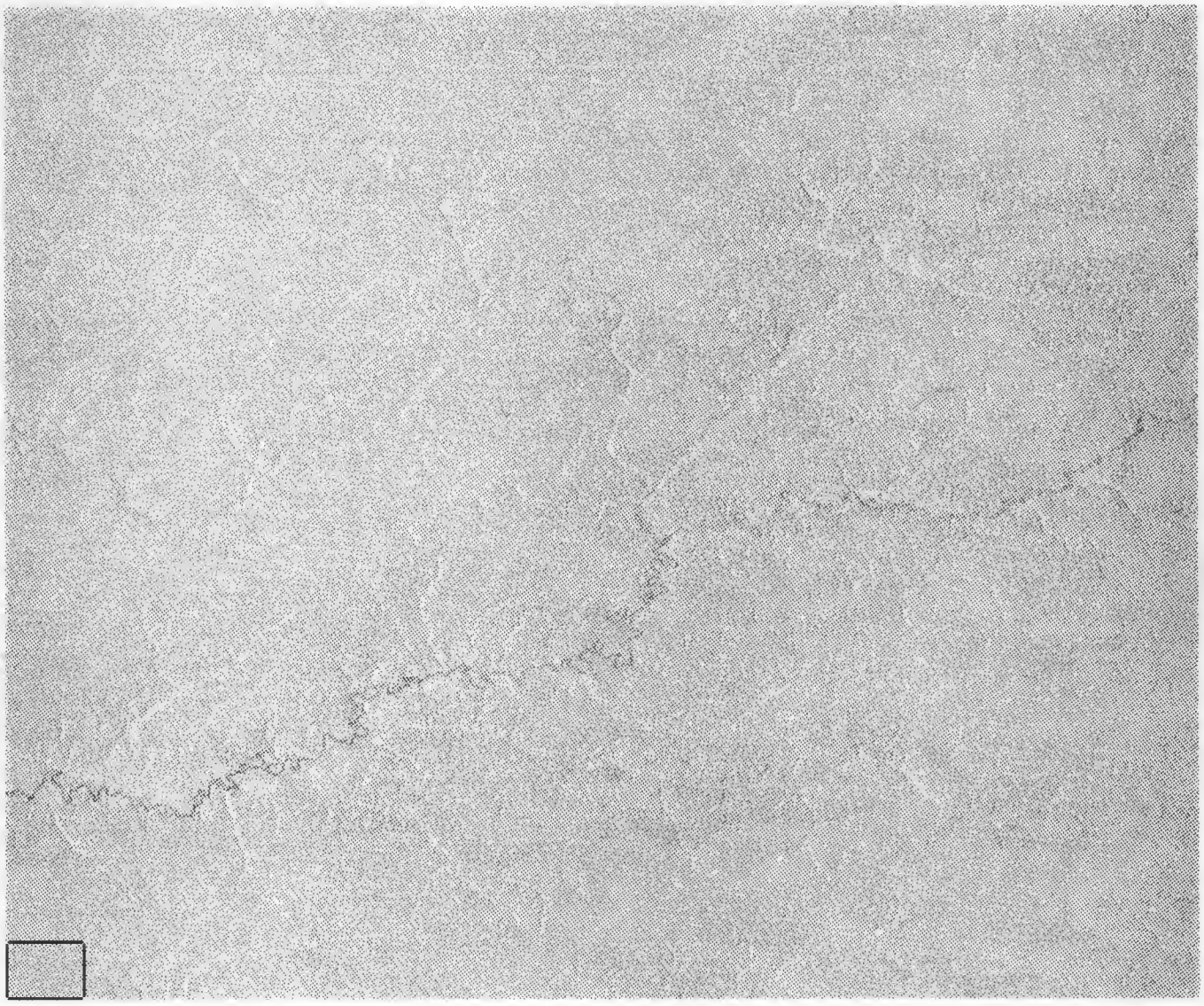

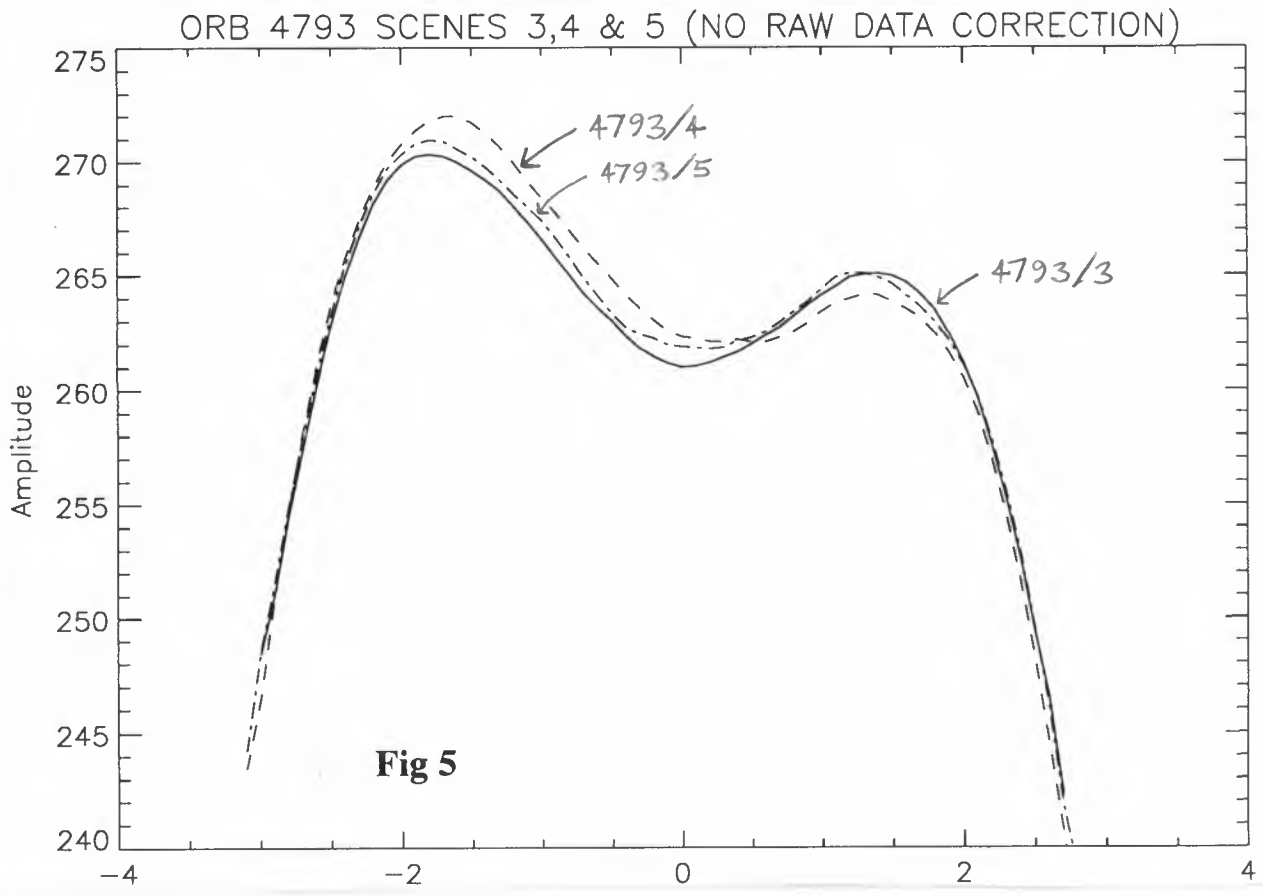
ORB 4793 SCENES 3,4 & 5 (NO RAW DATA CORRECTION)
Amplitude
275
270
265
260
255
250
245
240
−4
−2
0
2
4
4793/4
4793/5
4793/3

Fig 5

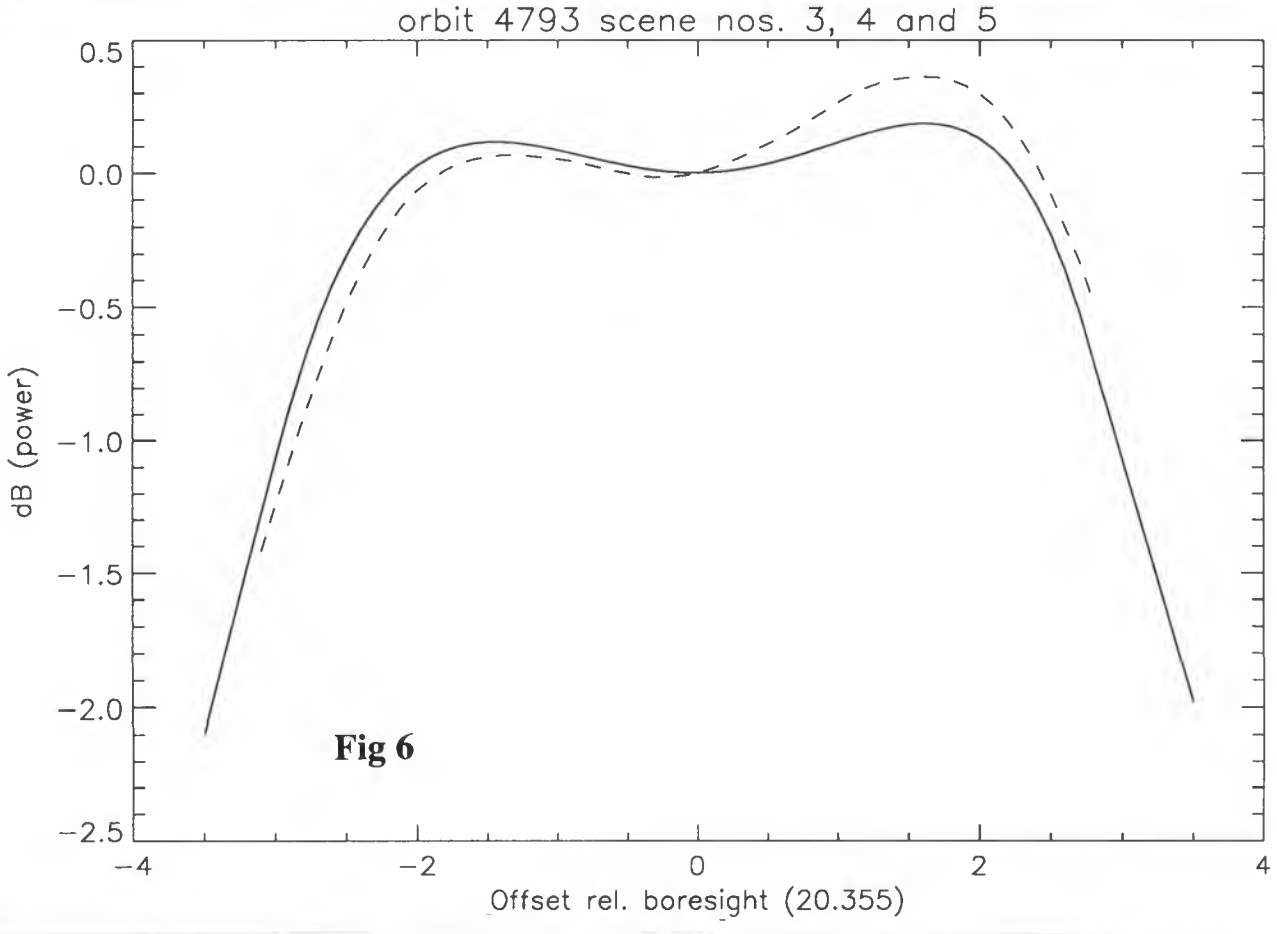
orbit 4793 scene nos. 3, 4 and 5
dB (power)
0.5
0.0
−0.5
−1.0
−1.5
−2.0
−2.5
−4
−2
0
2
4
Offset rel. boresight (20.355)

Fig 6

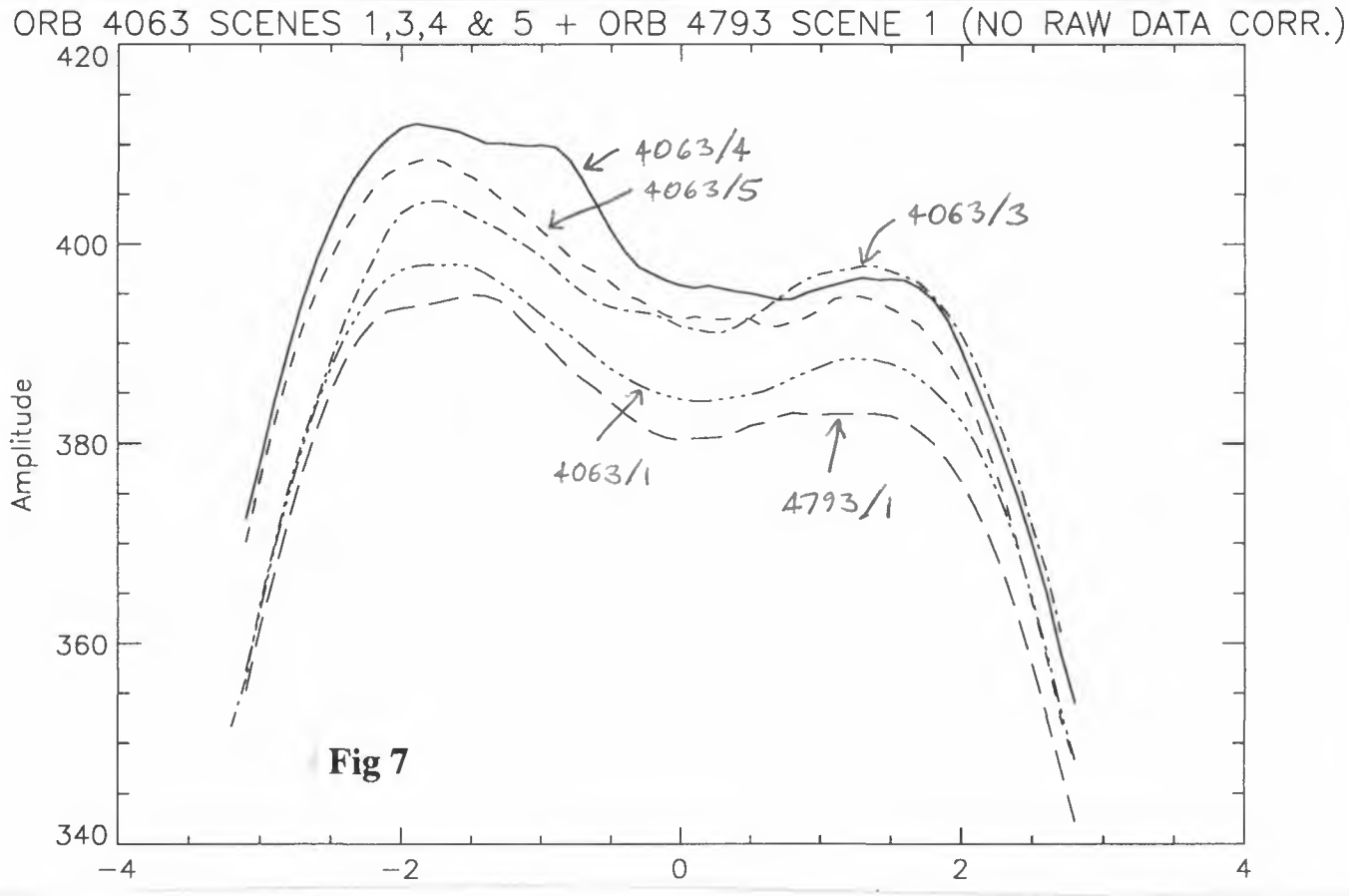
ORB 4063 SCENES 1,3,4 & 5 + ORB 4793 SCENE 1 (NO RAW DATA CORR.)
Amplitude
420
400
380
360
340
−4
−2
0
2
4
4063/4
4063/5
4063/3
4063/1
4793/1

Fig 7

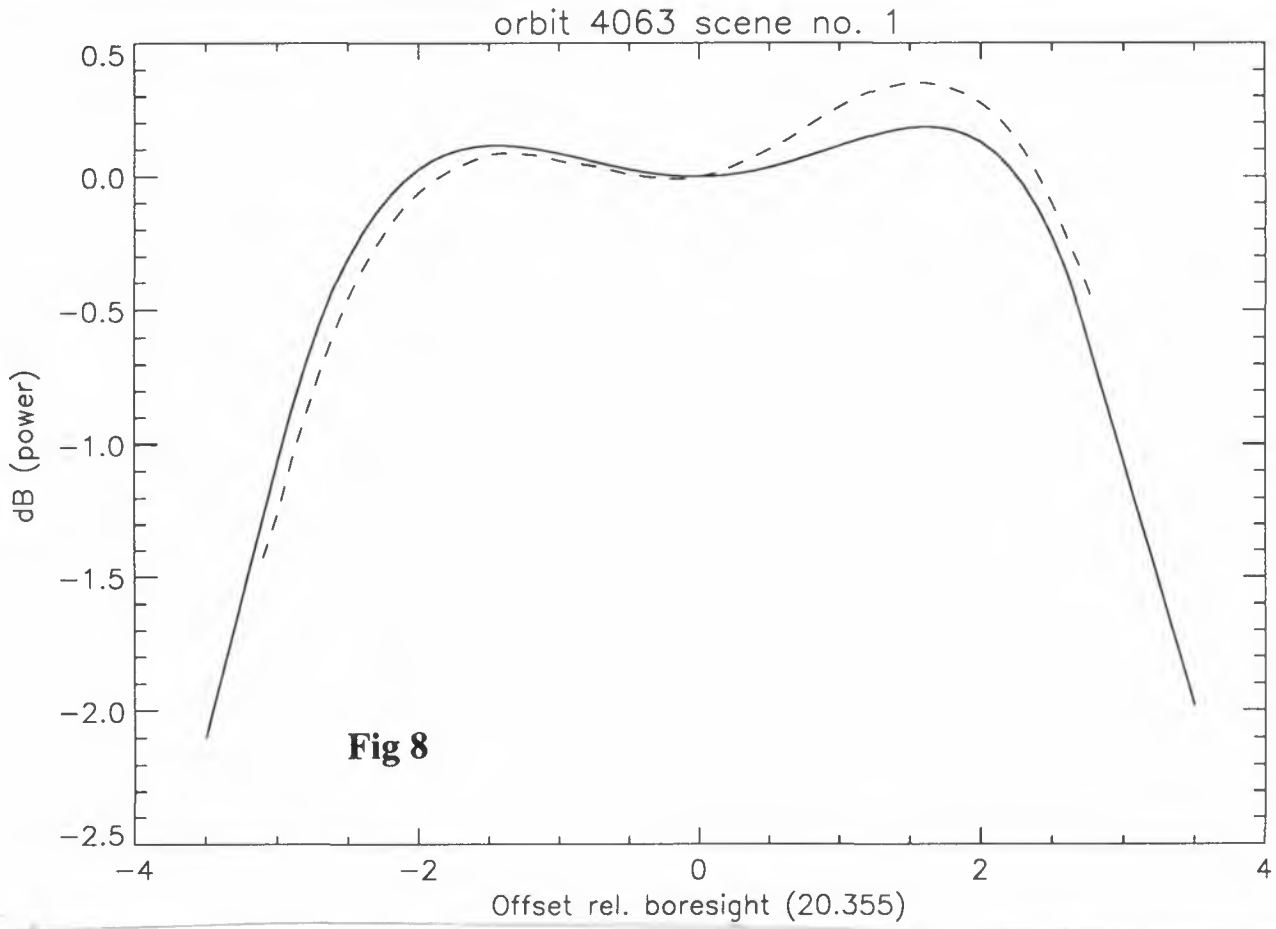
orbit 4063 scene no. 1
dB (power)
0.5
0.0
−0.5
−1.0
−1.5
−2.0
−2.5
−4
−2
0
2
4
Offset rel. boresight (20.355)

Fig 8

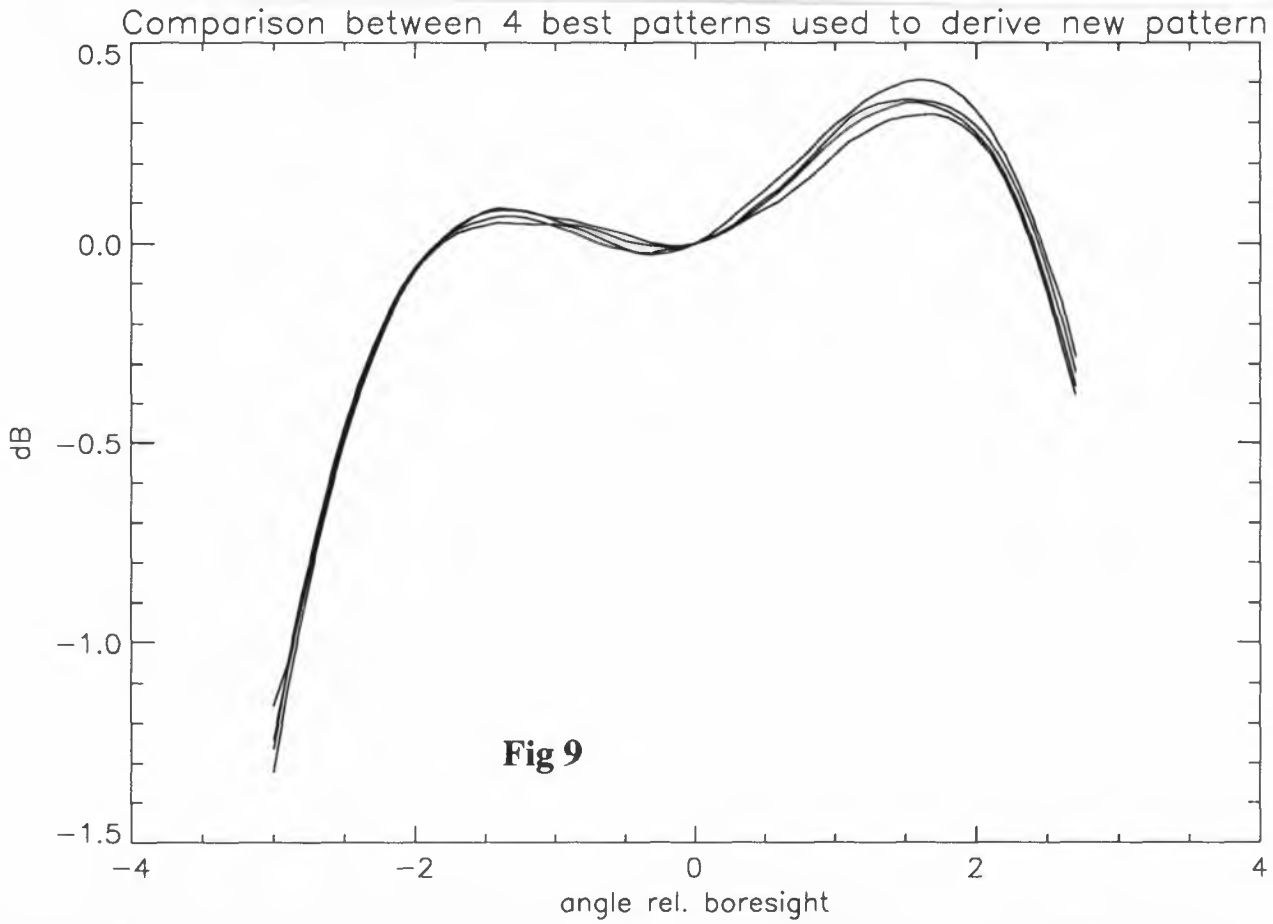
Comparison between 4 best patterns used to derive new pattern
0.5
0.0
−0.5
−1.0
−1.5
dB
−4
−2
0
2
4
angle rel. boresight

Fig 9

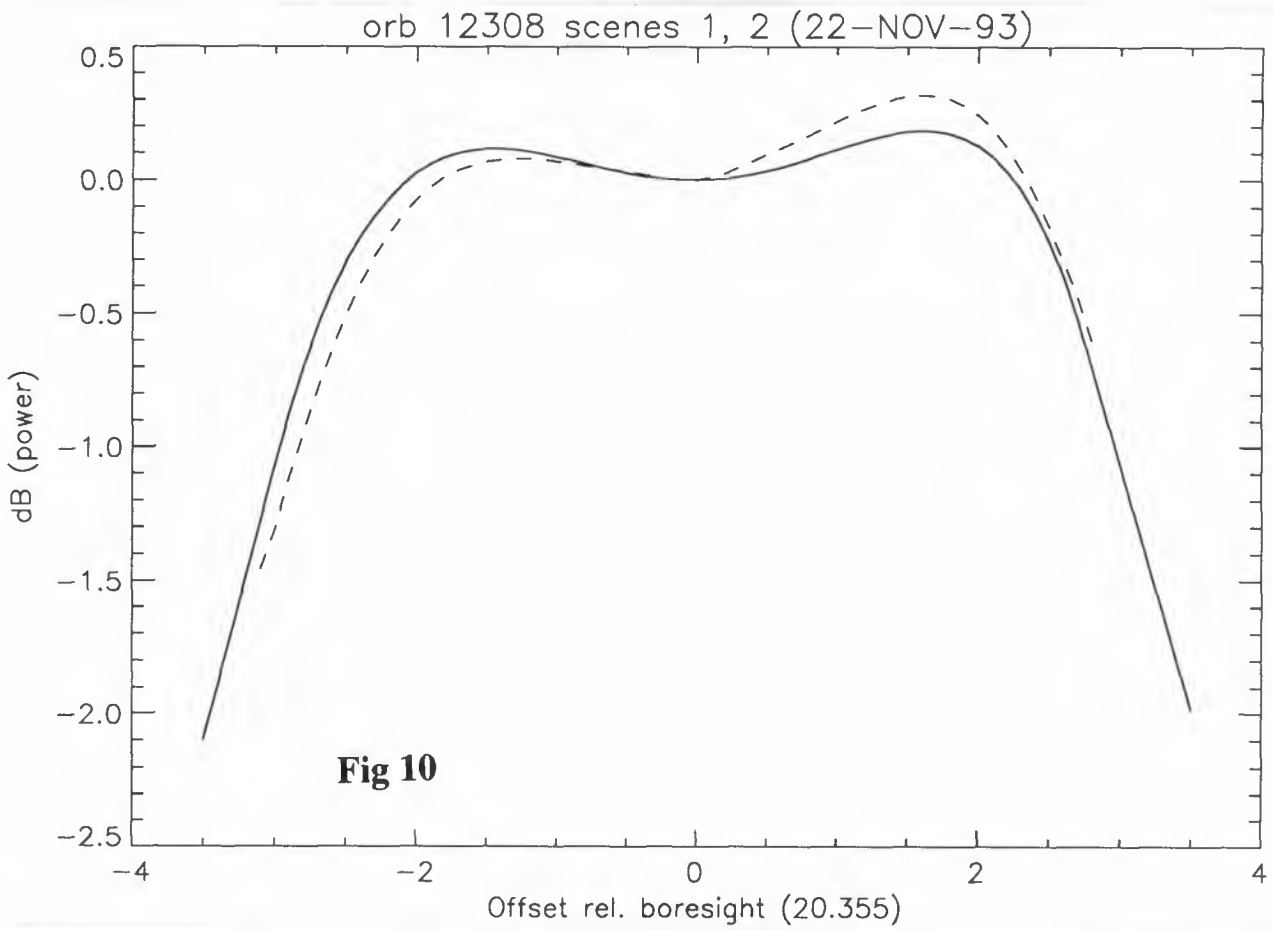
orb 12308 scenes 1, 2 (22−NOV−93)
0.5
0.0
−0.5
−1.0
−1.5
−2.0
−2.5
dB (power)
−4
−2
0
2
4
Offset rel. boresight (20.355)

Fig 10

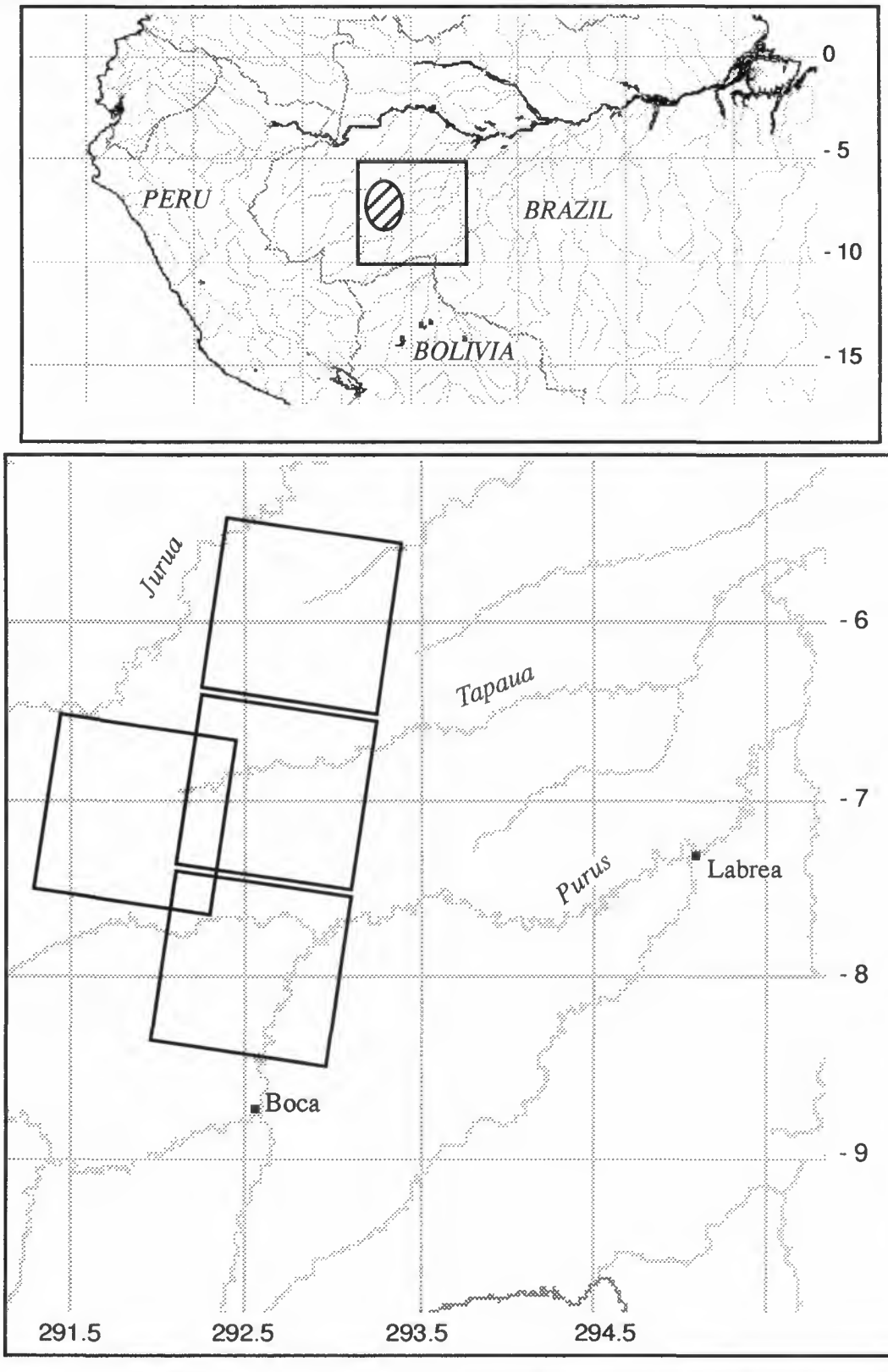

Fig 11 Location of the four selected scenes

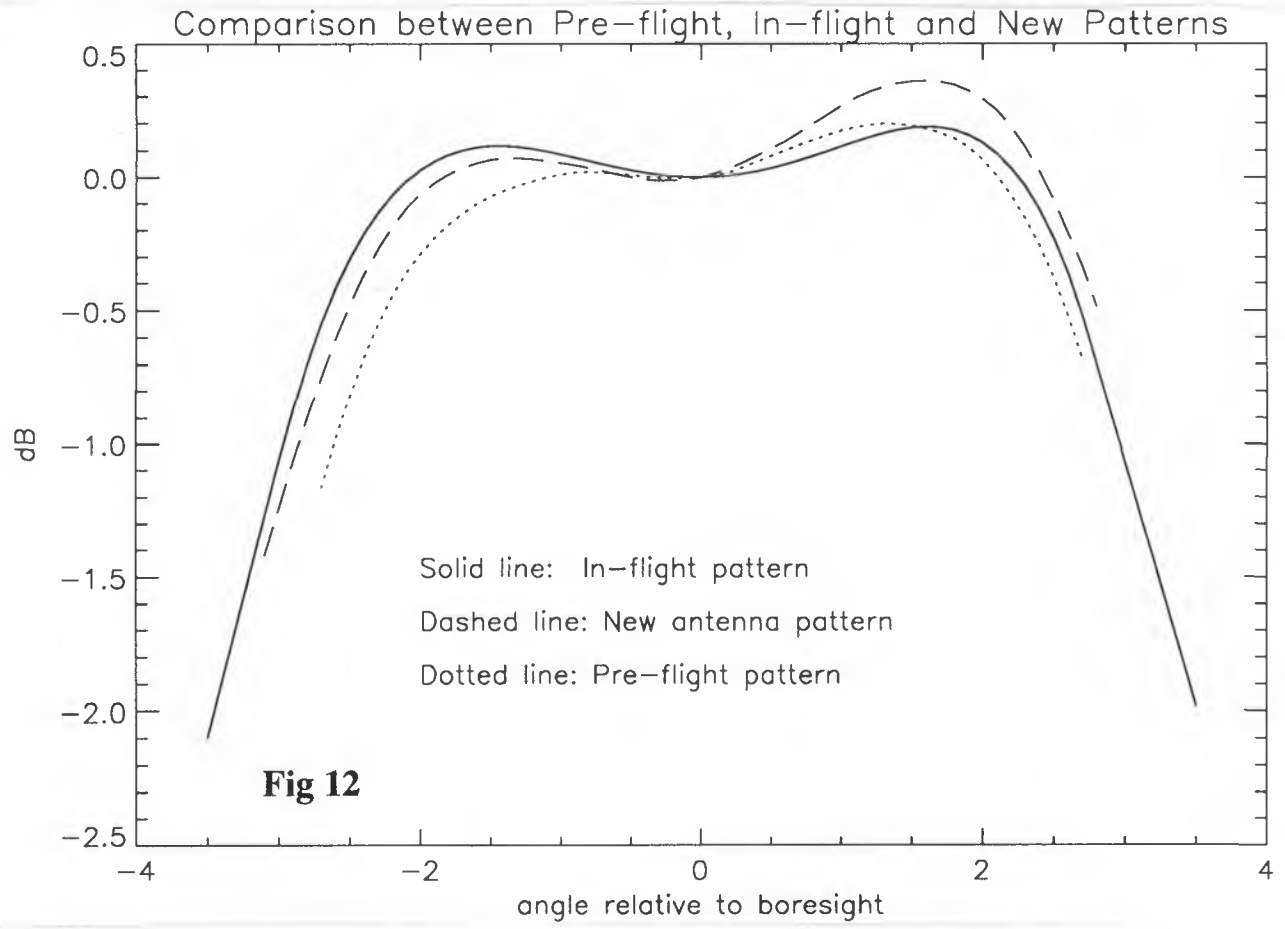
Comparison between Pre−flight, In−flight and New Patterns
0.5
0.0
−0.5
−1.0
−1.5
−2.0
−2.5
dB
−4
−2
0
2
4
angle relative to boresight
Solid line: In−flight pattern
Dashed line: New antenna pattern
Dotted line: Pre−flight pattern

Fig 12

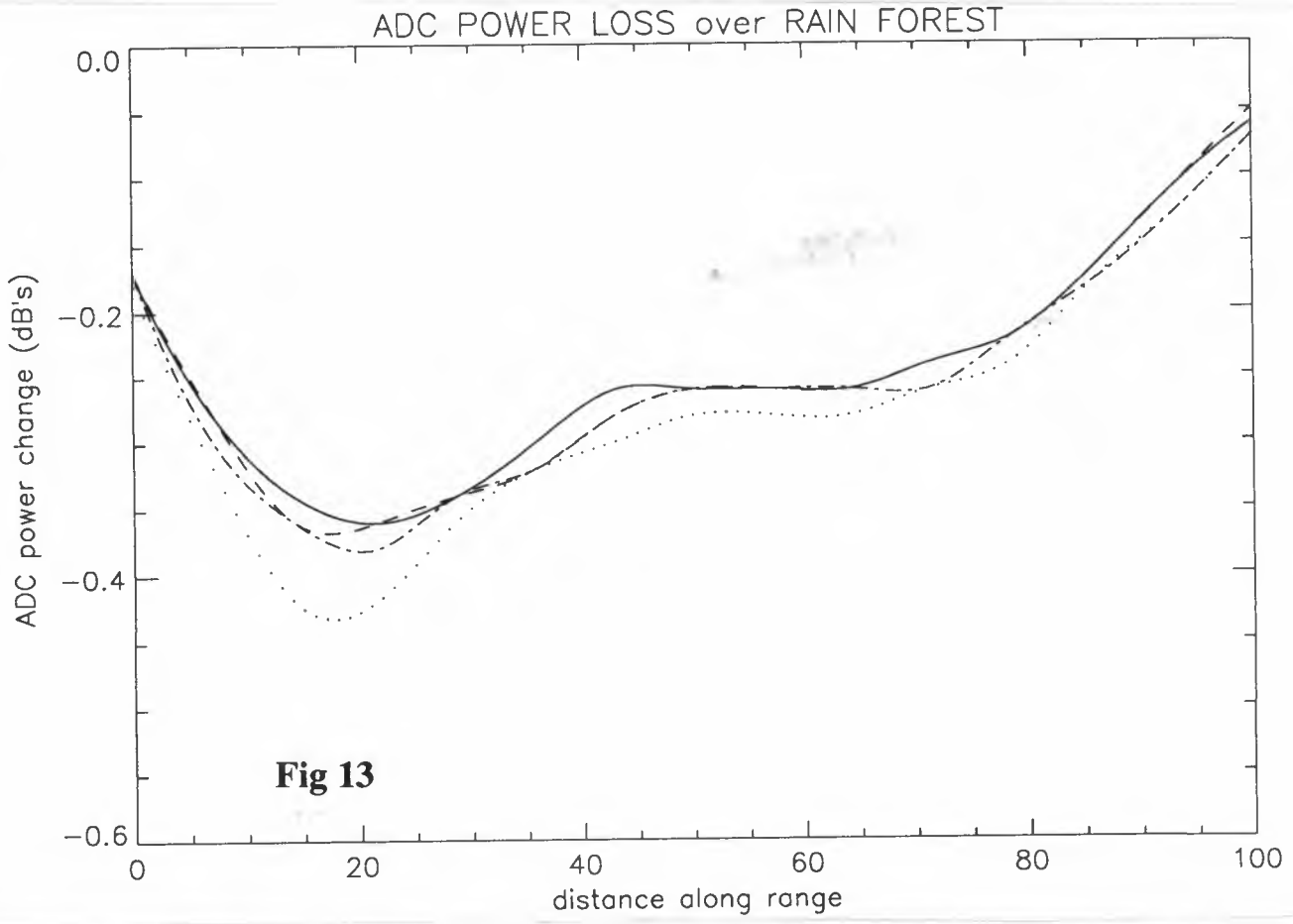
ADC POWER LOSS over RAIN FOREST
0.0
−0.2
−0.4
−0.6
ADC power change (dB's)
0
20
40
60
80
100
distance along range

Fig 13

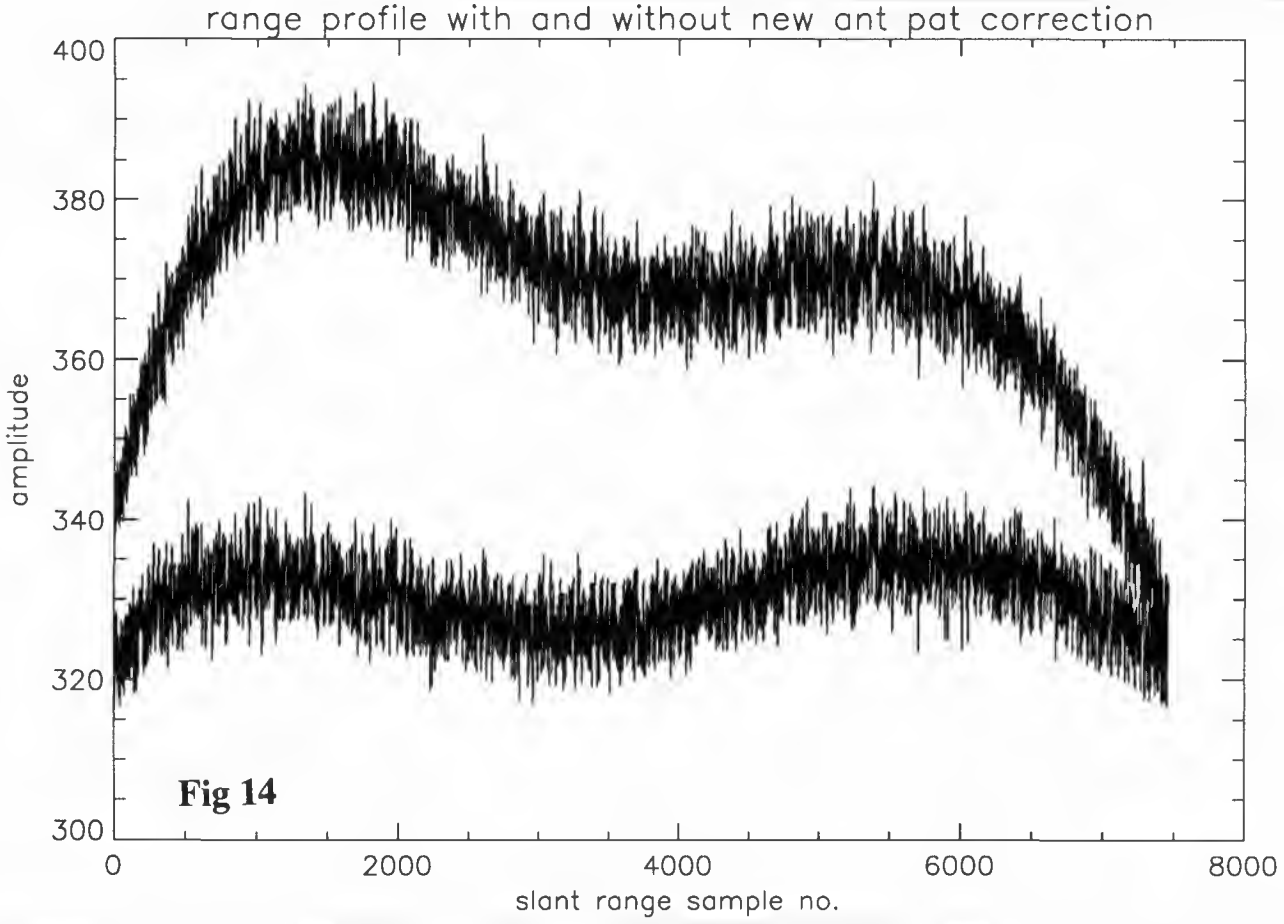
range profile with and without new ant pat correction
amplitude
400
380
360
340
320
300
0
2000
4000
6000
8000
slant range sample no.

Fig 14

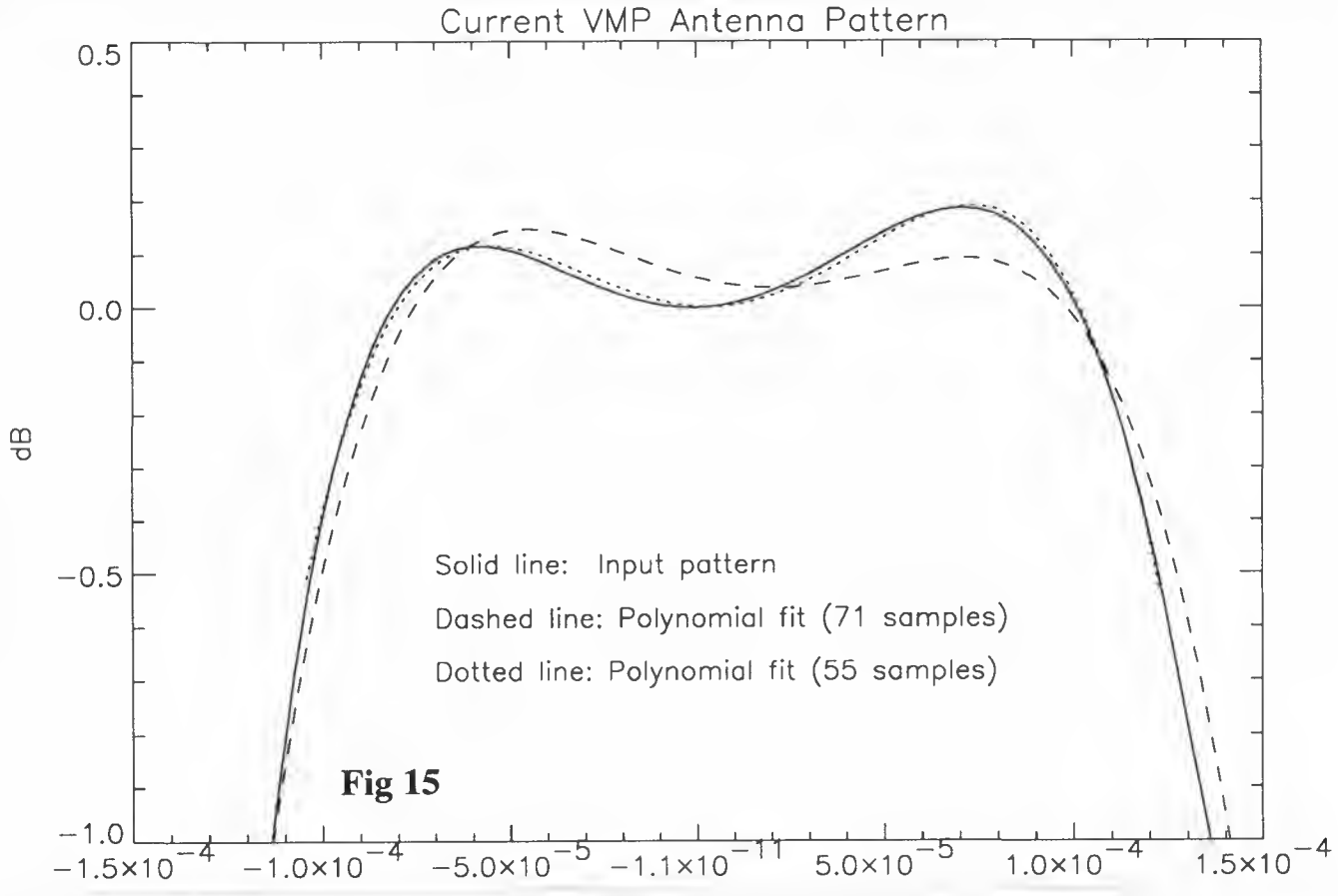
Current VMP Antenna Pattern
dB
0.5
0.0
−0.5
−1.0
−1.5×10−4
−1.0×10−4
−5.0×10−5
−1.1×10−11
5.0×10−5
1.0×10−4
1.5×10−4
Solid line: Input pattern
Dashed line: Polynomial fit (71 samples)
Dotted line: Polynomial fit (55 samples)

Fig 15

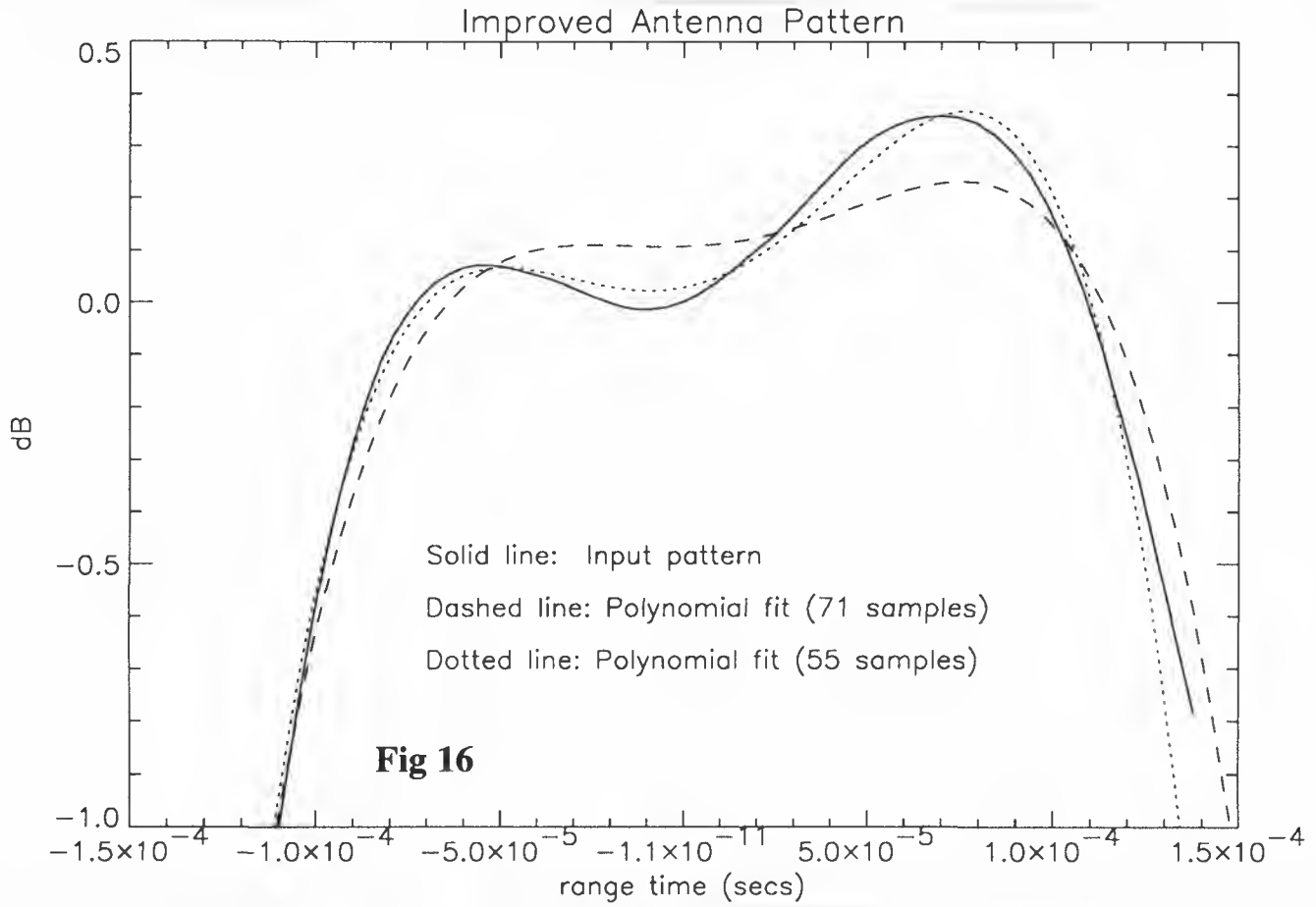

Fig 16

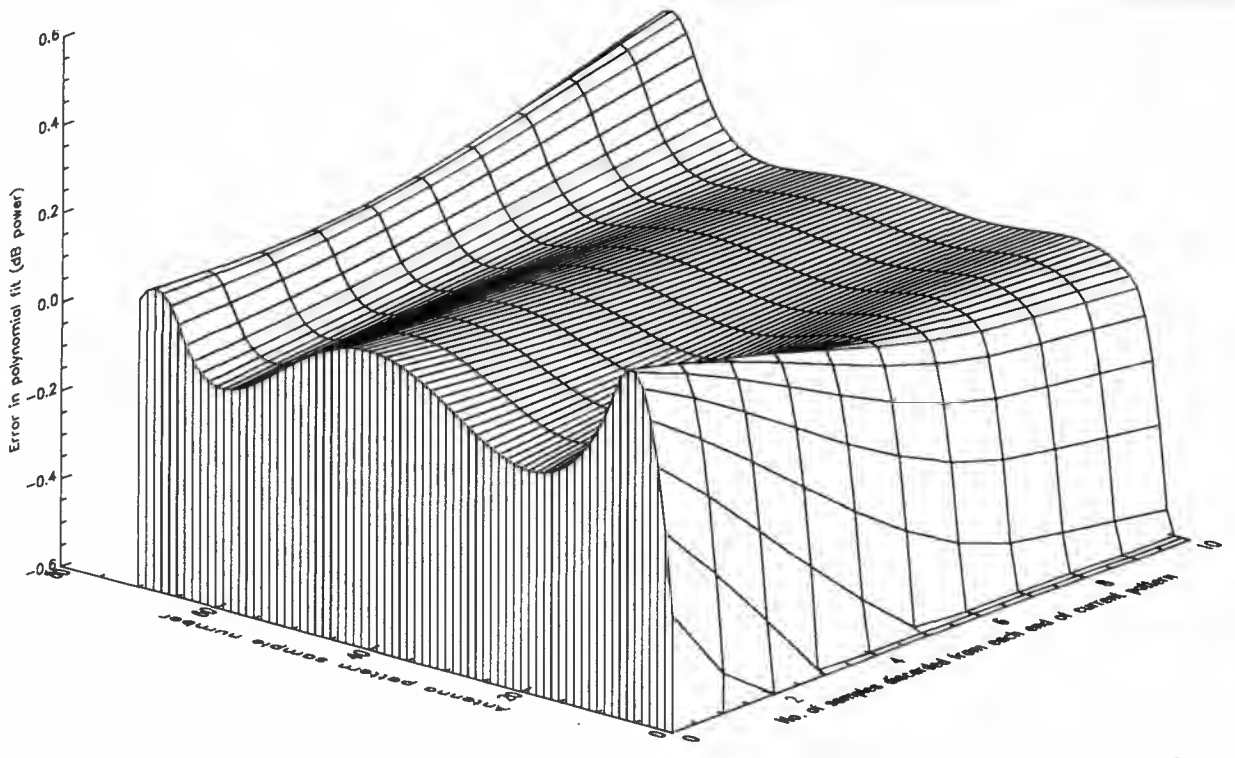

Fig 17 Poly Fit Error as a function of Input Length: Current Pattern

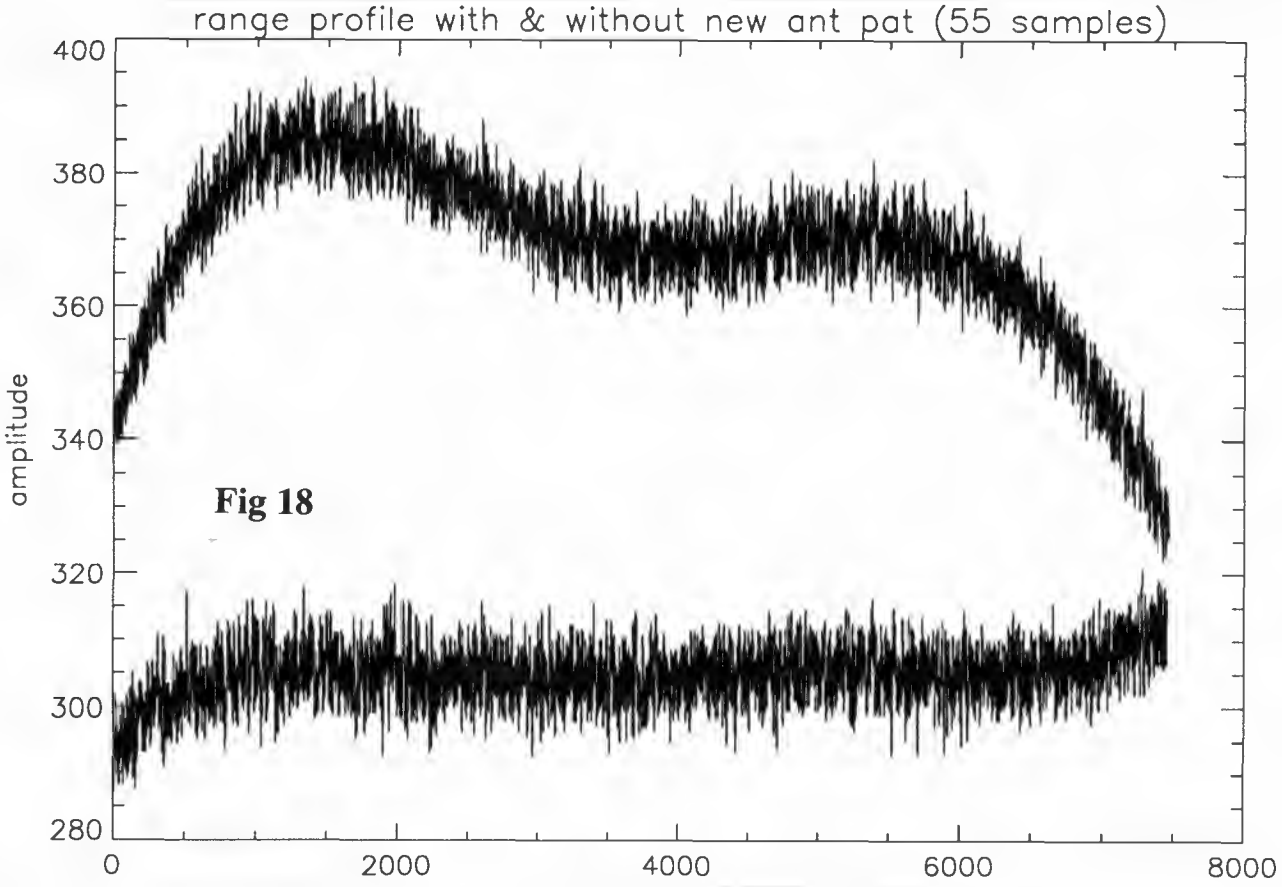

Fig 18

18

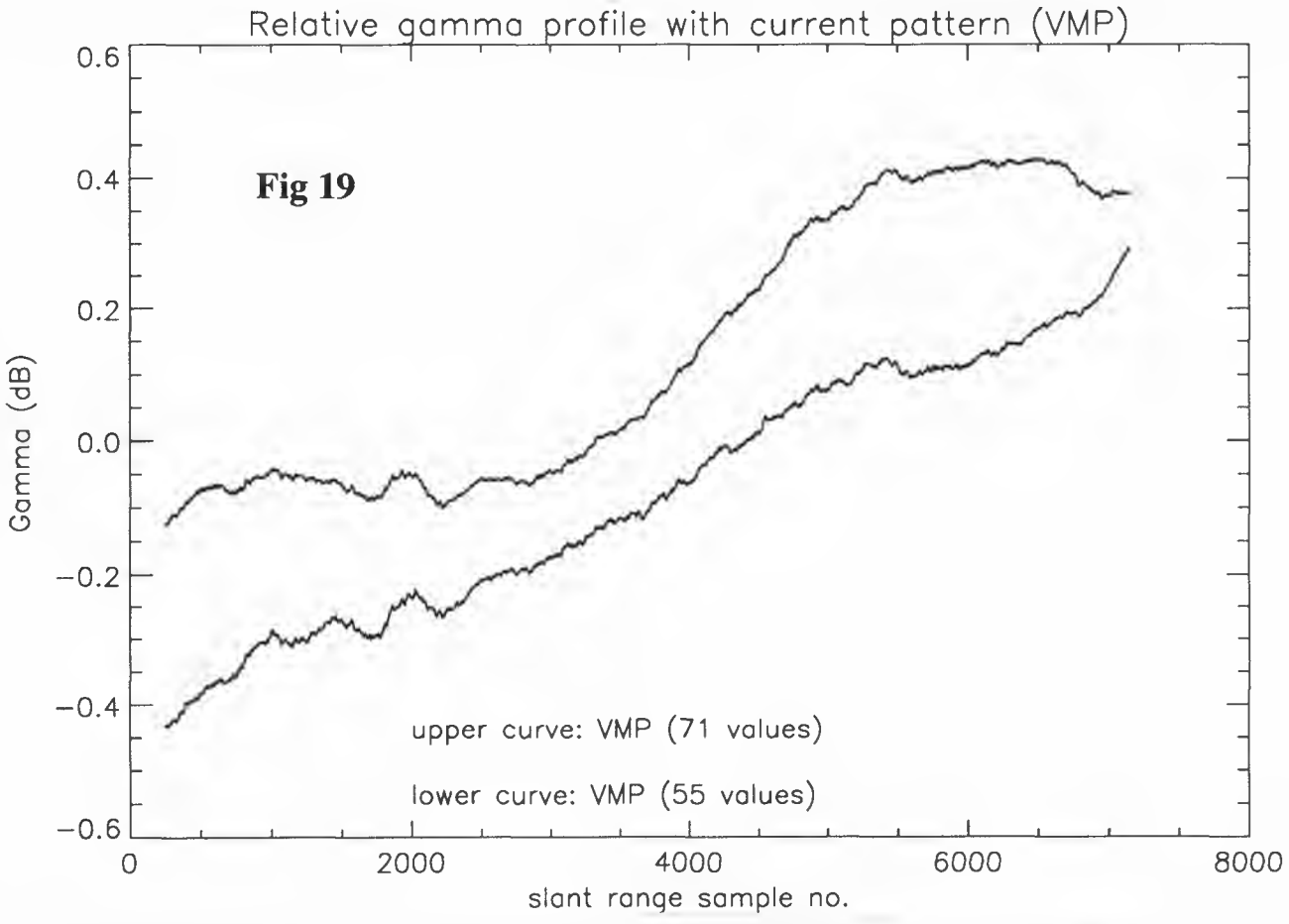

Fig 19

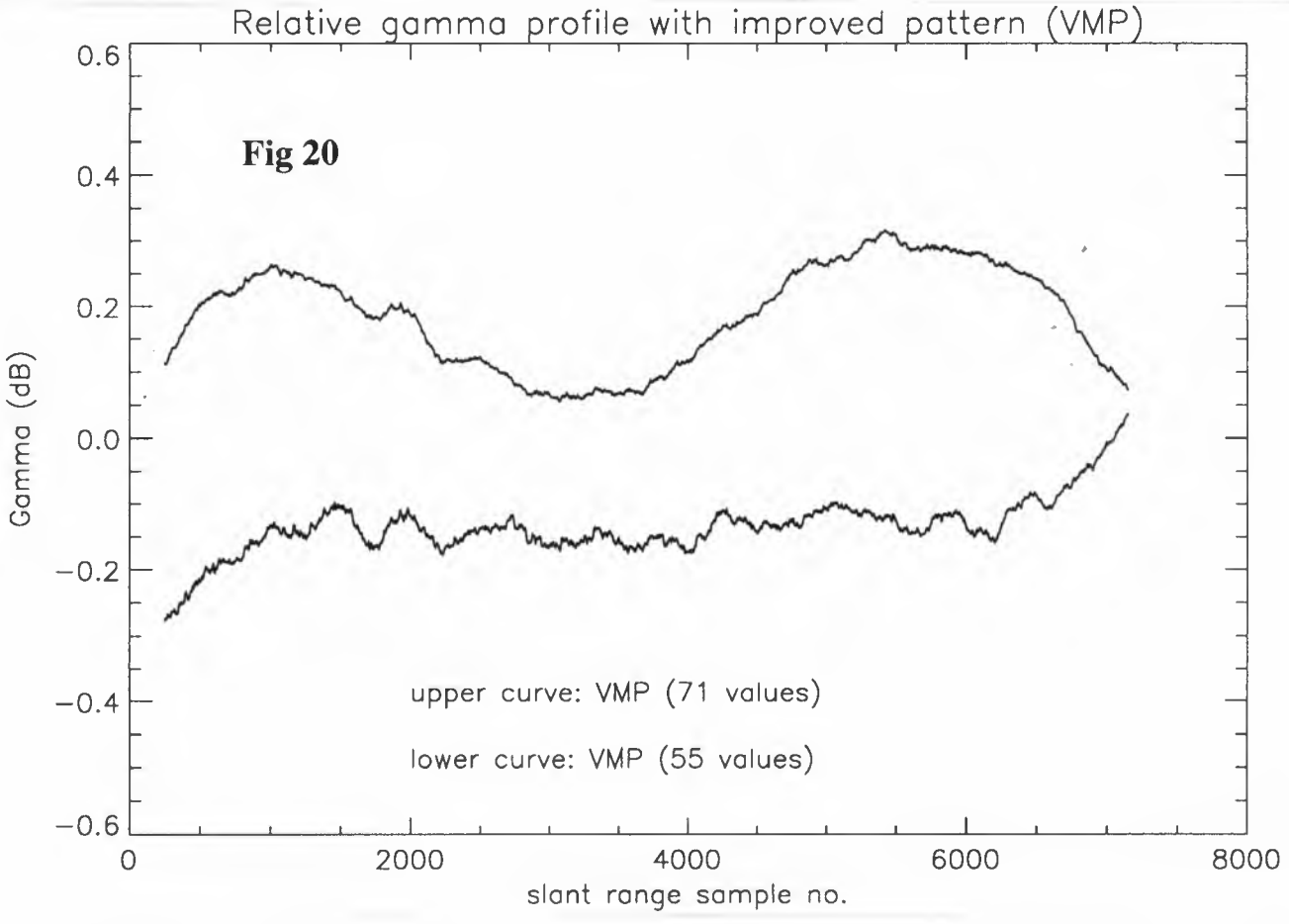
Relative gamma profile with improved pattern (VMP)
Fig 20
Gamma (dB)
0.6
0.4
0.2
0.0
−0.2
−0.4
−0.6
0
2000
4000
6000
8000
slant range sample no.
upper curve: VMP (71 values)
lower curve: VMP (55 values)

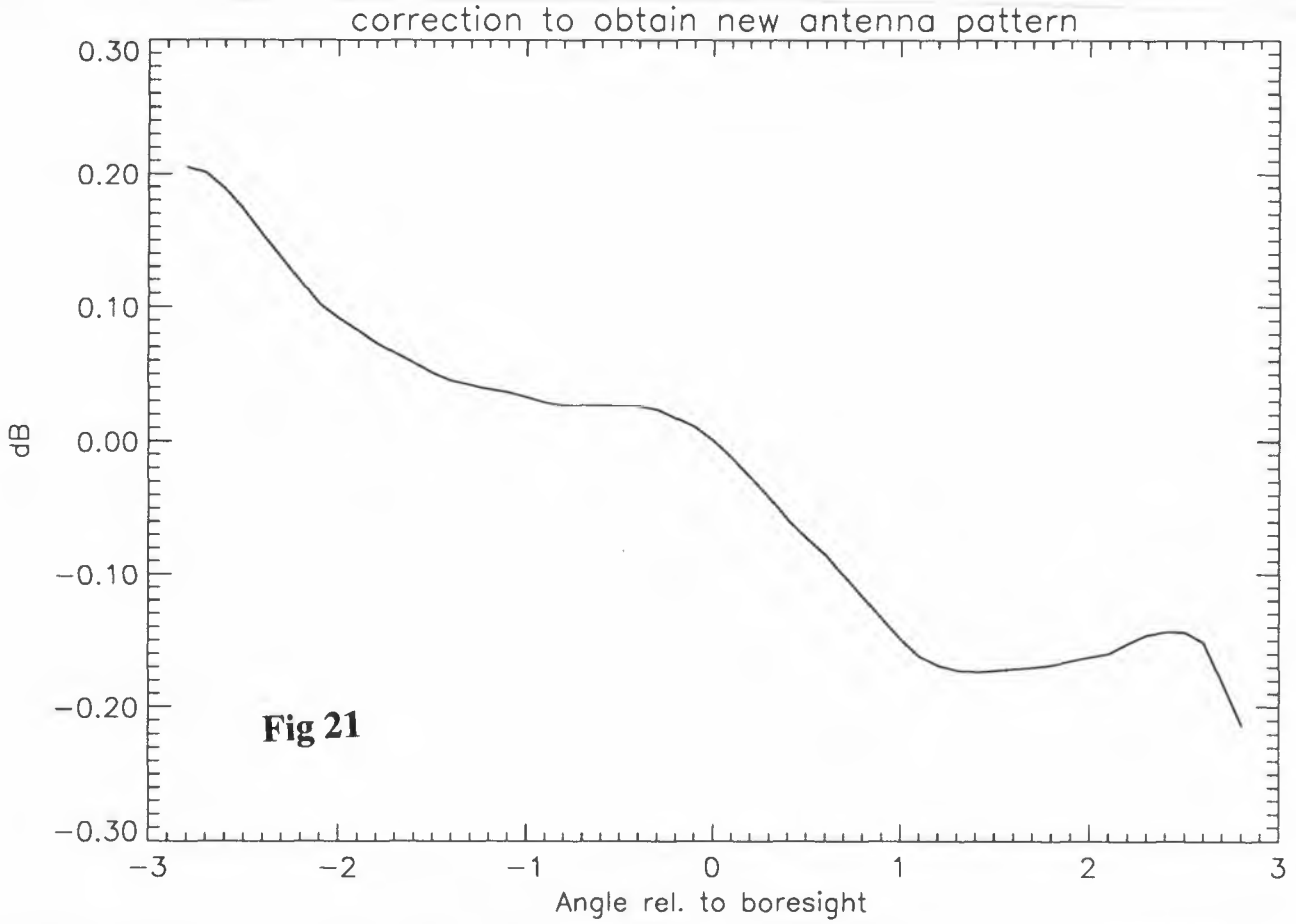
correction to obtain new antenna pattern
0.30
0.20
0.10
0.00
−0.10
−0.20
−0.30
dB
−3
−2
−1
0
1
2
3
Angle rel. to boresight

Fig 21

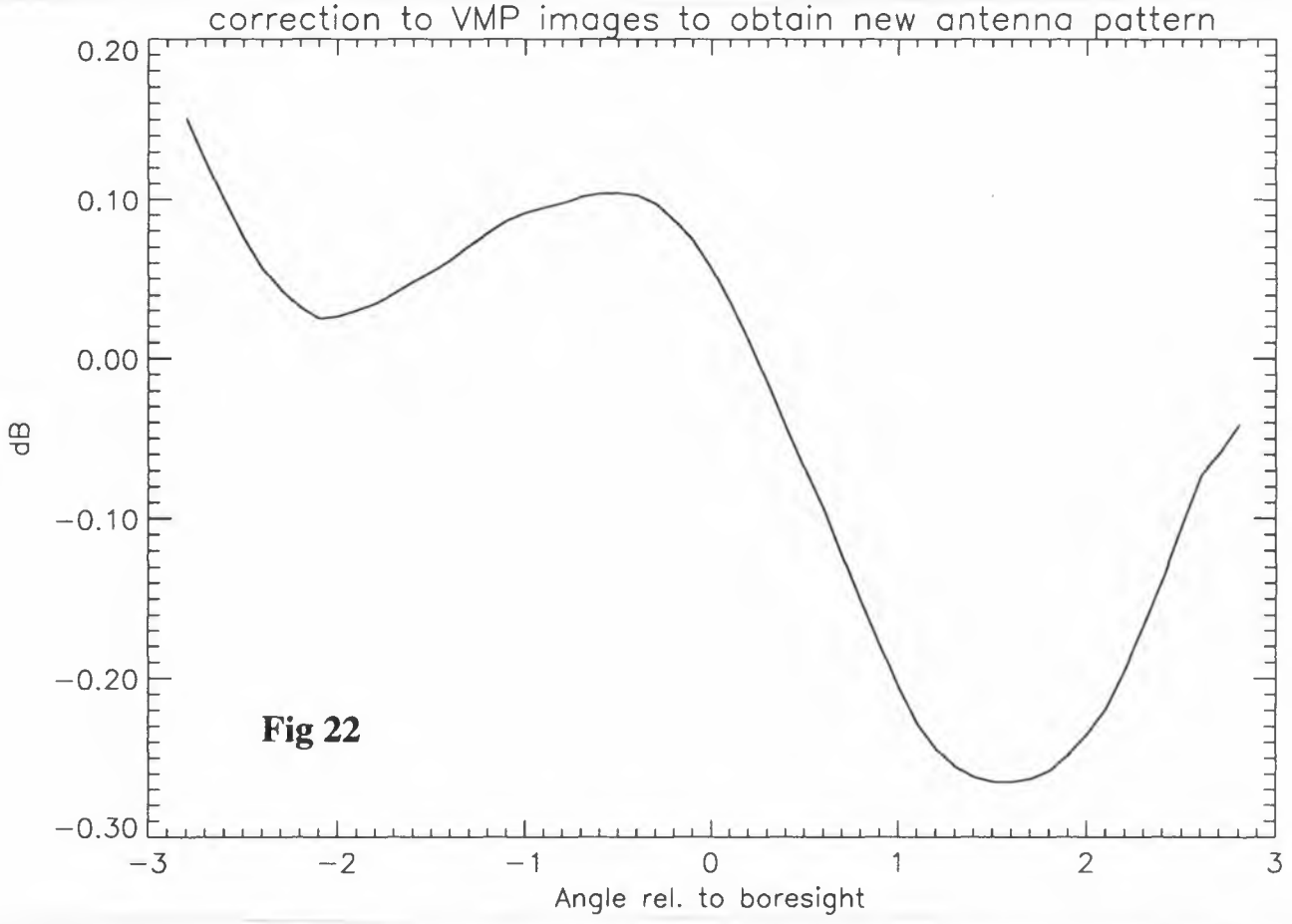
correction to VMP images to obtain new antenna pattern
0.20
0.10
0.00
−0.10
−0.20
−0.30
dB
−3
−2
−1
0
1
2
3
Angle rel. to boresight

Fig 22